ICARUS 73, 349–378 (1988)

Uranian Ring Orbits from Earth-Based and Voyager Occultation Observations

RICHARD G. FRENCH,*,[1] J. L. ELLIOT,*,† LINDA M. FRENCH,*,[2]
JULIE A. KANGAS,†,[2] KAREN J. MEECH,* AND MICHAEL E. RESSLER†,[3]

Department of Earth, Atmospheric, and Planetary Sciences, and †Department of Physics, Massachusetts Institute of Technology, Cambridge, Massachusetts 02139

MARC W. BUIE

Institute for Astronomy, 2680 Woodlawn Drive, Honolulu, Hawaii 96822

JAY A. FROGEL

Kitt Peak National Observatory, National Optical Astronomy Observatory, 950 North Cherry Avenue, Tucson, Arizona 85726

J. B. HOLBERG

Lunar and Planetary Laboratory, University of Arizona, Tucson, Arizona 85713

JESUS J. FUENSALIDA

Instituto de Astrofisica de Canarias, Universidad de la Laguna, S./C. de Tenerife, Islas Canarias, Spain

AND

MARSHALL JOY

Department of Astronomy, University of Texas–Austin, R. L. Moore Hall, Austin, Texas 78712

Received May 22, 1987; revised August 11, 1987

A new kinematical model for the Uranian rings has been determined from a combination of previously analyzed Earth-based stellar occultation data, three new stellar occultation data sets obtained in 1985 and 1987, and Voyager 2 occultation results. The new Earth-based occultations were of stars U23, U25, and U28 from the prediction list of Mink and Klemola (D. J. Mink and A. Klemola, 1985, *Astron. J.* 90, 1894–1899). The 4 May 1985 U23 occultation was observed from Cerro Tololo Interamerican Observatory (CTIO), McDonald Observatory, and Teide Observatory on Tenerife, and the 24 May 1985 U25 event was observed from CTIO, McDonald Observatory, and the IRTF on Mauna Kea. The 26 April 1987 U28 occultation was observed from the IRTF. Square-well models were fitted to the observed ring profiles to determine ring midtimes, widths, and optical depths. Voyager photopolarimeter and ultraviolet spectrometer observations of the σ Sgr and β Per stellar occultations provided strong constraints on the direction of the planetary pole

[1] Now at Department of Astronomy, Wellesley College, Wellesley, MA 02181.

[2] Guest Observer, Cerro Tololo Interamerican Observatory, La Serena, Chile.

[3] Now at Department of Physics and Astronomy, University of Hawaii, Honolulu, HI 96822.

0019-1035/88 $3.00

because of the oblique viewing geometry. Voyager radio science X-band occultation ring profiles observed with the Deep Space Station at Tidbinbilla were fitted with diffracted square-well models and strongly constrained the absolute radius scale of the ring system. The estimated accuracy of the new orbit solution is ±1 km in the semimajor axes of the rings, and ±0.01° in the direction of Uranus' pole. Rings 6, 5, 4, α, β, η, and ϵ were fitted to elliptical, inclined orbits precessing under the influence of the gravitational harmonics J_2 and J_4, with typical RMS ring plane residuals of a few hundred meters. The newly-discovered ring 1986U1R was fitted by a circular, equatorial model. The δ and γ rings are shown to have excited normal modes which cause them to deviate significantly (several kilometers in orbital radius) from simple ellipses. The γ ring exhibits an $m = 2$ distortion with a best-fitting pattern speed of 23.43821 ± 0.00004 deg hr^{-1}. The radius corresponding to an $m = 2$ normal mode with this pattern speed falls within 1 km of the newly fitted semimajor axis of the ring, confirming the suggestion of Porco and Goldreich (C. C. Porco and P. Goldreich, 1987, *Astron. J.* 93, 724–729) that the δ-ring shape distortion is due to an excitation of its $m = 2$ normal mode. The bizarre pattern of γ-ring observations is shown to be due to the combination of an $m = 1$ and an $m = 0$ mode; the entire precessing elliptical ring undergoes radial oscillations with a frequency of 47.73198 ± 0.00019 deg hr^{-1}. The amplitude of the oscillations is 5.15 ± 0.33 km, remarkably close to the amplitude $ae = 5.19 \pm 0.33$ km of the $m = 1$ mode which is also present in the γ ring. The resonance radius for the $m = 0$ mode is within 1 km of the fitted semimajor axis of the ring. A comparison of satellite resonance locations and fitted ring radii supports the suggestion of Porco and Goldreich (C. C. Porco and P. Goldreich, 1987, *Astron. J.* 93, 724–729) that 1986U7 is shepherding the outer edge of the δ ring and 1986U8 is shepherding the inner edge of the γ ring. The new orbit solution confirms their identification of the 24:25 outer eccentric resonance of 1986U7 with the inner edge of the ϵ ring, the 14:13 inner eccentric resonance of 1986U8 with the outer edge, and the likelihood that 1986U7 also shepherds 1986U1R.

I. INTRODUCTION

Prior to the Voyager 2 encounter with Uranus in January 1986, our knowledge of the Uranian rings was acquired primarily from Earth-based observations of over a dozen stellar occultations at visible and near-infrared wavelengths (see Elliot and Nicholson 1984, for a recent review). All of the nine "classical" rings have been observed at a variety of ring longitudes at a radial resolution of a few kilometers, limited primarily by diffraction. The long time-baseline, simultaneous coverage from separate stations and accurate event timing have made it possible to fit for the orbits of the rings (with an uncertainty in the absolute radius scale of about 5 km), the direction of the planetary pole, and the gravitational harmonics J_2 and J_4. We have learned that rings need not be circular and confined to the equatorial plane, as conventional wisdom once suggested, that narrow elliptical rings such as the ε ring can precess uniformly, resisting the tendency to be circularized by differential precession, and the the δ ring has an orbital distortion well matched by a Lindblad resonance (French *et al.* 1986b). From model fits to the observed ring profiles, variations of ring widths and mean opacity with ring longitude have also been determined, and it has been shown that the rings are not optical monolayers, but are many particles thick (French *et al.* 1986a).

The passage of Voyager 2 through the Uranian system provided important new information about the nature of the rings. Stunning images revealed previously unseen ring material, sheets of dust particles,

and a host of small satellites, two of which clearly play a central role in the dynamics and confinement of the rings (Smith *et al.* 1986, Porco and Goldreich 1987). Radio occultation observations having very high signal-to-noise ratio (Tyler *et al.* 1986) showed details of the radial structure at a resolution of tens of meters (L. Tyler and E. Marouf, personal communication), and ultraviolet spectrometer (UVS) and photopolarimeter (PPS) observations of the stellar occultations of σ Sgr and β Per recorded a newly discovered narrow ring, 1986U1R (Holberg *et al.* 1987, Lane *et al.* 1986).

This rich set of observations makes it possible to investigate in detail many of the dynamical puzzles posed by the rings, once a sufficiently accurate kinematical model of the system has been established. For example, the dynamics of ring structure and confinement are strongly suspected to involve resonances with shepherd satellites. Since the widths of the relevant resonances are quite narrow (a few kilometers—see Eq. (5) of Porco and Goldreich 1987), determining whether or not a given resonance will have an important effect on the rings requires that the orbits of the rings be determined to an accuracy of order 1 km. As another example, the existence of shepherd satellites too small to be seen in Voyager images might be inferred by slight perturbations they produce in the radial structure on the rings or by the anomalous precession they induce in the rings, once the mean structure and precession rates of the rings have been determined with sufficient accuracy.

With the goal of improving our understanding of ring structure and dynamics, we have combined an enhanced Earth-based occultation data set and Voyager occultation observations to determine a new solution for the ring orbital elements and the direction of the planetary pole. In the next two sections, we describe the new ground-based observations and the Voyager data used for this analysis. In Section IV, we discuss the new orbit solution, and in Section V we describe a search for resonances associated with the γ and δ rings, which are not well matched by simple elliptical orbits. Then, in Section VI, we discuss the new solution and investigate the suspected association of resonances between the satellites 1986U7 and 1986U8 and some of the rings (Porco and Goldreich 1987, Goldreich and Porco 1987). Finally, in the last section, we present our conclusions.

II. EARTH-BASED OBSERVATIONS AND DATA ANALYSIS

The most recent Uranus ring orbit model utilized all available observations through 1983 (French *et al.* 1986a). From trial orbit solutions with subsets of these data, it was evident that the radial scale of the rings and the pole direction could be obtained with much greater accuracy if multiple observations of several occultations from widely separated sites were available. Furthermore, it was clear that accurate absolute timing of all observations was essential in order to avoid potentially quite large systematic errors in the derived orbital elements and pole direction. In particular, a discrepancy between the timing of two sets of observations of the 22 April 1982 occultation of KME14 (Klemola *et al.* 1981) could not be resolved with the data available at the time. For these reasons, we carried out worldwide observations of two occultations on 4 May 1985 (U23) and 24 May 1985 (U25), taken from Table I of the occultation prediction list of Mink and Klemola (1985). These events were selected because both ingress and egress ring profiles could be observed over a north–south separation of several thousand kilometers and because near-infrared photometry of the occultation stars (French *et al.* 1985) showed that we could expect high signal-to-noise ratios. Subsequently, the 26 April 1986 occultation of U28 (Mink and Klemola 1985) was observed from a single station, the IRTF. Table I contains a summary of the circumstances of each observation, described in more detail below.

A. Observing Strategy

Our strategy for observing the U23 and U25 events was to minimize the systematic errors that plagued previous multiple-observation occultations by taking the following measures:

- All data were recorded digitally at high time resolution to avoid undersampling.
- Portable clocks were used to ensure that the data were recorded on a common time base.
- Chopping was avoided, whenever possible, to improve signal-to-noise ratio and to simplify data interpretation.
- Instrumental response functions were carefully measured, and time constants were kept as short as possible to reduce artificial smoothing of the data.
- Calibrations of the full signal level from the occultation star were performed before and after the occultation and between individual ring events, whenever possible.

Accurate occultation timing was a key objective, but experience has shown that the time services at many observations are not adequate for this purpose for two reasons. First, there is often a considerable (and variable) propagation delay in the case of radio time signals. Second, high-speed photometry software at some sites uses interrupt-driven computer clocks for data acquisition and timing, so the true sample time and duration are subject to unpredictable variations. To ensure that all observations utilized a common time base, accurate to the submillisecond level, portable clocks (designed by R. Baron) were used as the primary time reference at each observatory.

Three Vectron Laboratories FS321E and one Hewlett–Packard HP-105B oven-stabilized quartz oscillators, with battery backup power, were provided with circuitry to display UT digitally and to display any offset with respect to an external standard to an accuracy of ± 1 μsec. The frequency stability was tested in the laboratory and shown to be good to about 5×10^{-10} over several days. Each clock was calibrated and set, using the atomic clock at Haystack Observatory, prior to each occultation and again upon return from the field. As an additional check, the local time service at each observatory was compared with the portable clock time. Finally, 1-second pulses were recorded as part of the data stream, either throughout the occultation or before and after each occultation, in order to provide a direct time signal in the digitally recorded data. We estimate that the time base used for all the U23 and U25 observations agrees with UTC to better than 1 msec.

All observations were made in the infrared using a K filter (2.2 μm) to take advantage of the very low albedo of Uranus at this wavelength due to a strong methane absorption band.

B. Data Analysis Procedure

Ring event times for use in the orbit solution were obtained from square-well

TABLE I

EARTH-BASED OBSERVATIONS OF URANUS RING OCCULTATIONS

Date	Star	Station	Aperture (m)	Focal plane aperture (arcsec)	Observations (UTC)	Sample (sec)	Filter	Mode
4 May 1985	U23	CTIO	4.0	6	2:51:00–7:29:48	0.005	K	Chopped
		McDonald Obs.	2.7	10	5:26:01–6:33:29	0.005	K	DC
		Teide Obs.	1.5	25	3:50:00–5:43:20	0.005	K	DC
24 May 1985	U25	CTIO	4.0	6	7:10:00–8:54:18	0.002	K	DC
		McDonald Obs.	2.7	10	7:17:00–9:24:00	0.005	K	DC
		IRTF	3.0	10	7:15:00–9:34:00	0.005	K	Chopped
26 April 1986	U28	IRTF	3.0	10	13:11:41–15:41:01	0.0032	K	DC

TABLE II

EARTH-BASED OCCULTATION STARS—PHOTOMETRY AND DIAMETERS

Star	K	J–K	V–K	Angular diameter (milliarcsec)	Projected diameter (km)
U23	9.30 ± 0.10	0.93 ± 0.15	3.90 ± 0.20	0.151 ± 0.023	2.00 ± 0.30
U25	6.48 ± 0.10	1.24 ± 0.15	6.02 ± 0.20	0.324 ± 0.057	4.25 ± 0.75
U28	9.10 ± 0.02	−0.55 ± 0.04	4.91 ± 0.10	0.090 ± 0.019	1.20 ± 0.25

model fits to the data, including the effects of diffraction, finite stellar angular diameter, and instrumental response, as described by Elliot *et al.* (1984). The stellar angular diameter for each occultation was determined as follows. A square-well model was fitted to each of the narrowest ring profiles (typically, rings 6, 5, 4, η, γ, and δ), with the stellar angular diameter included as a free parameter. The adopted diameter was the average of the individual fitted diameters, each weighted inversely by the variance of the fit. The limb darkening parameter, b, was assumed to be equal to 1 in each case (see Elliot *et al.* 1984, Eq. (8)). Table II lists the results of this procedure, along with photometry of each star. The U23 and U25 photometry is taken from French *et al.* (1986), and the U28 photometry was obtained during the occultation observing run.

It was important to account for the finite response time of the detector and associated electronics, since the incoming signal during a ring occultation may vary quite rapidly, only to be smoothed (filtered) by the process of detection. At most stations, we recorded the instrumental response to a range of known inputs, from submillisecond square waves to step functions, using an infrared-light-emitting diode as an artificial light source driven by a pulse generator. At the other sites, we moved the aperture rapidly across a stellar image, either by slewing the telescope or by nodding the secondary, and recorded the approximate step response. We then fitted the observed response function, using a single- or double-pole filter function, as appropriate.

After the stellar diameter and instrumental response function were determined, each ring profile was then fitted using a square-well model, with the full stellar intensity and its uncertainty determined from calibrations prior to or during the occultation. The free parameters in each fit were the ring, width, midtime, fractional transmission f_0, and the background intensity level. Fits were also performed for two alternative measures of ring transmission: the equivalent depth A (defined as the ring width projected on the sky times the optical depth of the square-well model profile) and the equivalent width E (defined as $(1 - f_0)$ times the projected ring width). The fits using f_0, A, and E all converged to identical model curves, as one would expect because they are simply different means of representing the same square-well model. The fits using A and E were performed solely to determine the uncertainties in these quantities.

The formal errors in the fitted parameters given by the least-squares fitting procedure do not account for uncertainties in the stellar diameter, instrumental response function, and full stellar intensity level, since these were held fixed during each fit. French *et al.* (1986a) developed a scheme to estimate the errors associated with each of these and to add them in quadrature. We modified this procedure so that it could be automated on the computer. For each ring profile, a set of square-well fits was performed with the assumed values for the

TABLE III

RESULTS OF SQUARE-WELL RING PROFILE FITS TO 4 MAY 1985 OBSERVATIONS OF U23 FROM CTIO

Ring	Event	Midtime (UTC)	Width	Equivalent width E (km)	Equivalent depth A (km)	Fractional transmission f_0	Normal optical depth	True anomaly (deg)
6	I	5:08:11.470 ± 0.003	1.73 ± 0.54	{0.69 ± 0.01}	{0.89 ± 0.06}	{0.60 ± 0.09}	[0.51]	128.1
6	E	5:54:30.437 ± 0.002	1.07 ± 0.02	[0.53]	[0.74]	(0.50)	[0.69]	55.0
5	I	5:07:33.631 ± 0.001	2.52 ± 0.05	{1.38 ± 0.01}	{2.00 ± 0.04}	{0.45 ± 0.02}	[0.79]	110.2
5	E	5:55:03.262 ± 0.001	0.98 ± 0.10	{0.94 ± 0.06}	{3.50 ± 0.82}	{0.03 ± 0.04}	[3.58]	35.8
4	I	5:07:09.560 ± 0.001	1.21 ± 0.42	{0.92 ± 0.17}	{1.75 ± 0.68}	{0.23 ± 0.19}	[1.45]	12.3
4	E	5:55:38.212 ± 0.001	2.63 ± 0.06	{1.15 ± 0.01}	{1.51 ± 0.02}	{0.56 ± 0.01}	[0.58]	296.8
α	I	5:03:59.145 ± 0.001	4.02 ± 0.05	{3.22 ± 0.01}	{6.61 ± 0.17}	{0.19 ± 0.01}	[1.65]	318.4
α	E	5:58:50.129 ± 0.001	9.26 ± 0.04	{4.71 ± 0.03}	{6.62 ± 0.05}	{0.49 ± 0.01}	[0.71]	235.9
β	I	5:02:36.318 ± 0.002	11.56 ± 0.05	{3.37 ± 0.02}	{4.00 ± 0.03}	{0.71 ± 0.01}	[0.35]	167.9
β	E	6:00:07.066 ± 0.002	9.25 ± 0.04	{3.38 ± 0.02}	{4.22 ± 0.03}	{0.63 ± 0.01}	[0.46]	82.7
η	I	5:00:34.882 ± 0.003	1.38 ± 1.06	{0.55 ± 0.24}	[0.70]	{0.60 ± 0.60}	[0.51]	100.5
η	E	6:02:09.958 ± 0.003	3.06 ± 0.15	{0.79 ± 0.02}	{0.92 ± 0.02}	{0.74 ± 0.01}	[0.30]	11.4
γ	I	4:59:59.417 ± 0.001	4.52 ± 0.05	{3.81 ± 0.01}	{8.54 ± 0.24}	{0.15 ± 0.01}	[1.89]	10.2
γ	E	6:02:45.783 ± 0.001	3.38 ± 0.06	{3.09 ± 0.01}	{8.66 ± 0.64}	{0.08 ± 0.02}	[2.56]	280.0
δ	I	4:59:05.969 ± 0.001	6.08 ± 0.04	{3.22 ± 0.02}	{4.60 ± 0.04}	{0.47 ± 0.01}	[0.76]	246.1
δ	E	6:03:38.113 ± 0.001	2.73 ± 0.06	{2.26 ± 0.02}	{4.88 ± 0.22}	{0.17 ± 0.02}	[1.78]	154.3
ε	I	4:55:59.254 ± 0.001	23.37 ± 0.02	{21.37 ± 0.04}	{59.36 ± 0.52}	{0.08 ± 0.01}	[2.54]	10.7
ε	E	6:07:12.118 ± 0.002	58.31 ± 0.05	{43.28 ± 0.16}	{79.91 ± 0.63}	{0.25 ± 0.01}	[1.37]	273.3

Note. I and E stand for ingress and egress, respectively. Numbers in parentheses were held fixed during the fit. Numbers in square brackets were derived from other parameters in the fit. Numbers in braces were derived from separate fits and are alternative representations of the transparency of the ring. See text for discussion of errors.

stellar diameter, time constant, and stellar flux changed, in turn, by $\pm 1\sigma$, for a total of six additional fits. The error we adopted for each of the *fitted* parameters was either the formal error from the standard fit or the maximum difference between the fitted value from the standard fit and the six auxiliary fits, whichever was larger. (This procedure is, in principle, less rigorous than the previous method because errors from all sources are not added in quadrature. As a practical matter, this is not a problem since in nearly every case the error from one source dominates all others. For example, the fitted widths and equivalent depths of the narrow rings depend most sensitively on the adopted stellar diameter, and the equivalent depths of the wide rings depend most sensitively on the uncertainty in the stellar flux.)

Having described in general terms our observing and analysis methods, we turn now to a more detailed description of each of the new Earth-based observations. The results of the square-well model fits are given in Tables III–X. In each of these tables, quantities in square brackets were derived from other parameters in the fit, and quantities in parentheses were held fixed during the fit. In some cases, f_0 could not be fitted because of strong correlations with other fitted parameters. In other cases (principally in the auxiliary fits used to account for uncertainties in the full stellar intensity level), the fitted value of f_0 was negative, corresponding to an unphysical situation where the ring absorbs more than the available light. In these instances, the fractional transmission was fixed at zero, corresponding to infinite normal optical depth, and hence infinite equivalent depth, A. Because of the logarithmic relation between f_0 and A, the computed error in f_0 is finite while the error in A is infinite.

C. The 4 May 1985 Occultation of U23

We successfully observed the occultation of U23 from Cerro Tololo, McDonald Observatory, and Teide Observatory. P. Nicholson (private communication) reports that the event was also recorded from Mt. Palomar at high air mass. The stellar diameter of

TABLE IV

RESULTS OF SQUARE-WELL RING PROFILE FITS TO 4 MAY 1985 OBSERVATIONS OF U23 FROM MCDONALD OBSERVATORY

Ring	Event	Midtime (UTC)	Width (km)	Equivalent width E (km)	Equivalent depth A (km)	Fractional transmission f_0	Normal optical depth	True anomaly (deg)
6	Egress	6:02:42.501 ± 0.017	0.71 ± 0.18	[0.35]	[0.49]	(0.50)	[0.69]	44.6
5	Egress	6:03:09.448 ± 0.004	1.79 ± 0.13	{1.67 ± 0.19}	{4.95 ± 4.14}	{0.06 ± 0.06}	[2.76]	25.5
4	Egress	6:03:39.675 ± 0.007	2.74 ± 0.34	{1.18 ± 0.19}	{1.54 ± 0.36}	{0.57 ± 0.07}	[0.56]	286.7
α	Egress	6:06:22.569 ± 0.004	9.58 ± 0.13	{5.95 ± 0.96}	{9.36 ± 3.06}	{0.37 ± 0.10}	[0.98]	226.7
β	Egress	6:07:28.909 ± 0.006	8.91 ± 0.18	{4.73 ± 0.78}	{6.78 ± 1.87}	{0.46 ± 0.09}	[0.76]	73.9
η	Egress	6:09:17.461 ± 0.014	4.88 ± 0.51	{1.00 ± 0.17}	{1.12 ± 0.21}	{0.79 ± 0.03}	[0.23]	3.1
γ	Egress	6:09:49.447 ± 0.003	2.39 ± 0.08	[2.36]	[∞]	(0.00)	[∞]	271.9
δ	Egress	6:10:36.294 ± 0.003	3.73 ± 0.15	{3.16 ± 0.39}	{7.15 ± 4.04}	{0.14 ± 0.10}	[1.91]	146.3
ε	Egress	6:13:53.853 ± 0.004	62.63 ± 0.13	{56.63 ± 7.00}	[151.26]	{0.09 ± 0.11}	[2.42]	266.0

Note. Numbers in parentheses were held fixed during the fit. Numbers in square brackets were derived from other parameters in the fit. Fit for fractional transmission did not converge for rings 6 and γ. Numbers in braces were derived from separate fits and are alternative representations of the transparency of the ring. See text for discussion of errors.

U23 (Table II) was determined from a combination of narrow-ring square-well model fits to the Cerro Tololo and McDonald Observatory data. Selected profiles of the α, δ, and ε rings are included in Figs. 1, 2, and 3.

Cerro Tololo. Observations of both ingress and egress were obtained at the Cerro Tololo Interamerican Observatory (CTIO) under partially cloudy conditions. The data were recorded using the infrared photometer in the chopping mode with a 41 Hz chop and a $f/30$ chopping secondary. The response of the system had nonlinearities at time scales of several seconds, which should have little effect for the analyses done in this paper. Guiding was done with an on-axis TV viewing system. The electronic filter was set to the 12 db/octave mode, with a nominal time constant of 0.030 sec. The actual instrumental response was satisfactorily modelled using a double-pole filter function with a time constant of 0.034 sec. The results of the profile fits are given in Table III.

McDonald Observatory. Only the egress profiles were observable from McDonald Observatory; ingress occurred before Uranus rose above the horizon. Observations were made with a cooled InSb detector with a 10^{11}-ohm feedback resistor. The amplifier signal was input to a voltage-to-frequency converter and recorded digitally with a portable data system as described by Baron *et al.* (1983). The sky was clear, but quite bright because of scattered moonlight. The event was tracked continuously using a bright guide star due south of the

TABLE V

RESULTS OF SQUARE-WELL RING PROFILE FITS TO 4 MAY 1985 OBSERVATIONS OF U23 FROM TEIDE OBSERVATORY

Ring	Event	Midtime (UTC)	Width (km)	Equivalent width E (km)	Equivalent depth A (km)	Fractional transmission f_0	Normal optical depth	True anomaly (deg)
α	Ingress	4:54:10.569 ± 0.034	5.17 ± 1.08	{3.14 ± 0.67}	{4.85 ± 1.60}	{0.39 ± 0.14}	[0.94]	329.5
γ	Ingress	4:50:46.322 ± 0.021	3.47 ± 0.81	{3.04 ± 0.55}	{7.45 ± 4.34}	{0.11 ± 0.18}	[2.15]	20.2
δ	Ingress	4:49:59.739 ± 0.033	3.81 ± 1.41	{2.22 ± 0.64}	{3.34 ± 1.34}	{0.41 ± 0.20}	[0.88]	255.8
ε	Ingress	4:47:14.150 ± 0.019	23.83 ± 0.60	{22.34 ± 1.25}	{69.25 ± 24.15}	{0.05 ± 0.06}	[2.90]	19.7

Note. Numbers in square brackets were derived from other parameters in the fit. Numbers in braces were derived from separate fits and are alternative representations of the transparency of the ring. See text for discussion of errors.

TABLE VI

RESULTS OF SQUARE-WELL RING PROFILE FITS TO 24 MAY 1985 OBSERVATIONS OF U25 FROM CTIO

Ring	Event	Midtime (UTC)	Width (km)	Equivalent width E (km)	Equivalent depth A (km)	Fractional transmission f_0	Normal optical depth	True anomaly (deg)
6	I	8:00:59.288 ± 0.001	1.46 ± 0.84	{0.76 ± 0.03}	{1.07 ± 0.29}	{0.48 ± 0.24}	[0.73]	68.4
6	E	8:34:20.511 ± 0.001	1.61 ± 0.90	{0.72 ± 0.03}	{0.96 ± 0.25}	{0.55 ± 0.26}	[0.60]	4.7
5	I	8:00:27.393 ± 0.001	2.21 ± 0.67	{1.43 ± 0.03}	{2.33 ± 0.73}	{0.35 ± 0.19}	[1.05]	52.4
5	E	8:34:51.746 ± 0.001	1.82 ± 0.69	{1.27 ± 0.05}	{2.20 ± 0.92}	{0.29 ± 0.19}	[1.21]	347.2
4	I	7:59:58.286 ± 0.001	2.80 ± 0.74	{1.23 ± 0.01}	{1.63 ± 0.22}	{0.56 ± 0.15}	[0.58]	316.3
4	E	8:35:27.476 ± 0.001	3.43 ± 0.53	{1.31 ± 0.01}	{1.65 ± 0.10}	{0.62 ± 0.07}	[0.48]	249.4
α	I	7:57:07.905 ± 0.001	7.09 ± 0.10	{4.58 ± 0.06}	{7.43 ± 0.24}	{0.35 ± 0.02}	[1.05]	271.2
α	E	8:38:16.845 ± 0.002	10.59 ± 0.06	{5.43 ± 0.06}	{7.65 ± 0.13}	{0.48 ± 0.01}	[0.72]	196.3
β	I	7:55:57.769 ± 0.002	11.27 ± 0.05	{3.51 ± 0.03}	{4.22 ± 0.05}	{0.69 ± 0.01}	[0.37]	124.0
β	E	8:39:22.795 ± 0.001	7.16 ± 0.08	{3.41 ± 0.04}	{4.64 ± 0.11}	{0.52 ± 0.01}	[0.65]	46.1
η	I	7:54:11.746 ± 0.003	1.01 ± 1.14	{0.55 ± 0.04}	{0.79 ± 0.13}	{0.45 ± 0.27}	[0.79]	61.3
η	E	8:41:10.873 ± 0.003	2.80 ± 0.60	{0.85 ± 0.03}	{1.02 ± 0.07}	{0.69 ± 0.09}	[0.37]	338.9
γ	I	7:53:41.250 ± 0.001	1.84 ± 0.06	{1.82 ± 0.07}	[∞]	(0.00)	[∞]	332.2
γ	E	8:41:42.219 ± 0.001	2.15 ± 0.45	{2.13 ± 0.15}	[∞]	(0.00)	[∞]	248.7
δ	I	7:52:55.298 ± 0.001	5.22 ± 0.19	{3.37 ± 0.04}	{5.45 ± 0.29}	{0.35 ± 0.03}	[1.04]	209.9
δ	E	8:42:27.226 ± 0.001	2.71 ± 0.47	{2.04 ± 0.33}	{3.84 ± 1.34}	{0.24 ± 0.14}	[1.42]	124.5
ε	I	7:50:14.798 ± 0.001	20.80 ± 0.03	[20.60]	[∞]	(0.00)	[∞]	340.9
ε	E	8:45:41.608 ± 0.003	70.52 ± 0.10	{51.14 ± 0.31}	{92.03 ± 1.14}	{0.27 ± 0.01}	[1.31]	249.1

Note. I and E stand for ingress and egress, respectively. Numbers in parentheses were held fixed during the fit. Numbers in square brackets were derived from other parameters in the fit. Numbers in braces were derived from separate fits and are alternative representations of the transparency of the ring. Fractional transmission of γ-ring and ε-ring ingress profiles could not be reliably determined from the fits. See text for discussion of errors.

occultation star. Calibration of the signal from the occultation star was impeded by variations in the observed count rate after the dewar was refilled with LN_2, and we estimate that the adopted value is uncertain by about 10%. The time constant of the

TABLE VII

RESULTS OF SQUARE-WELL RING PROFILE FITS TO 24 MAY 1985 OBSERVATIONS OF U25 FROM MCDONALD OBSERVATORY

Ring	Event	Midtime (UTC)	Width (km)	Equivalent width E (km)	Equivalent depth A (km)	Fractional transmission f_0	Normal optical depth	True anomaly (deg)
6	I	7:57:57.631 ± 0.003	2.46 ± 0.79	{0.70 ± 0.02}	{0.83 ± 0.08}	{0.71 ± 0.14}	[0.34]	81.7
6	E	8:42:49.572 ± 0.004	0.78 ± 1.58	{0.50 ± 0.17}	[0.80]	{0.36 ± 0.40}	[1.02]	350.9
5	I	7:57:33.631 ± 0.002	2.56 ± 0.60	{1.32 ± 0.03}	{1.86 ± 0.32}	{0.48 ± 0.15}	[0.73]	65.4
5	E	8:43:12.991 ± 0.002	1.88 ± 0.76	{1.11 ± 0.03}	{1.70 ± 0.50}	{0.40 ± 0.21}	[0.90]	333.6
4	I	7:57:13.002 ± 0.003	3.16 ± 0.72	{1.07 ± 0.03}	{1.31 ± 0.09}	{0.66 ± 0.10}	[0.41]	329.0
4	E	8:43:40.126 ± 0.003	3.76 ± 0.50	{1.06 ± 0.03}	{1.39 ± 0.05}	{0.69 ± 0.05}	[0.37]	236.2
α	I	7:54:59.772 ± 0.001	6.27 ± 0.14	{3.75 ± 0.05}	{5.74 ± 0.19}	{0.40 ± 0.02}	[0.92]	282.5
α	E	8:45:52.056 ± 0.002	10.69 ± 0.07	{4.87 ± 0.05}	{6.53 ± 0.10}	{0.54 ± 0.01}	[0.61]	184.5
β	I	7:54:02.319 ± 0.005	11.51 ± 0.18	{3.12 ± 0.06}	{3.64 ± 0.07}	{0.73 ± 0.01}	[0.32]	134.7
β	E	8:46:45.214 ± 0.002	6.91 ± 0.10	{3.23 ± 0.05}	{4.37 ± 0.11}	{0.53 ± 0.01}	[0.63]	34.8
η	I	7:52:34.651 ± 0.007	3.30 ± 0.68	{0.65 ± 0.04}	{0.72 ± 0.05}	{0.80 ± 0.05}	[0.22]	72.4
η	E	8:48:14.736 ± 0.007	3.51 ± 0.72	{0.82 ± 0.05}	{0.94 ± 0.06}	{0.76 ± 0.06}	[0.27]	329.3
γ	I	7:52:08.993 ± 0.001	2.27 ± 0.57	{1.98 ± 0.13}	[4.81]	{0.12 ± 0.16}	[2.12]	342.0
γ	E	8:48:41.245 ± 0.001	2.51 ± 0.54	{2.07 ± 0.07}	{4.48 ± 3.13}	{0.16 ± 0.14}	[1.79]	238.1
δ	I	7:51:30.046 ± 0.002	5.35 ± 0.18	{3.07 ± 0.04}	{4.60 ± 0.18}	{0.42 ± 0.03}	[0.86]	219.5
δ	E	8:49:19.122 ± 0.002	2.41 ± 0.62	{1.66 ± 0.04}	{2.85 ± 0.86}	{0.30 ± 0.16}	[1.18]	114.4
ε	I	7:49:12.372 ± 0.001	20.81 ± 0.04	{19.33 ± 0.14}	{57.22 ± 2.57}	{0.06 ± 0.01}	[2.75]	349.7
ε	E	8:52:10.282 ± 0.002	76.44 ± 0.08	{50.63 ± 0.32}	{83.64 ± 0.96}	{0.33 ± 0.01}	[1.09]	239.9

Note. I and E stand for ingress and egress, respectively. Numbers in square brackets were derived from other parameters in the fit. Numbers in braces were derived from separate fits and are alternative representations to the transparency of the ring. Fits for equivalent depth had very large error bars for the ring 6 egress and γ-ring ingress profiles. See text for discussion of errors.

TABLE VIII

RESULTS OF SQUARE-WELL RING PROFILE FITS 24 MAY 1985 OBSERVATIONS OF U25 FROM IRTF

Ring	Event	Midtime (UTC)	Width (km)	True anomaly (deg)
ε	Egress	8:54:56.327 ± 0.007	78.67 ± 0.26	242.2

detector and electronics was determined to be 0.042 sec fitting a single-pole filter response function to the signal from a star slewed rapidly across the aperture. Table IV contains the results of the square-well profile fits.

Teide Observatory. The occultation ingress was observed using the infrared photometer on the 1.5-m telescope (TCS) at Tenerife; egress occurred after sunrise and was not observed. The time constant of the detector and electronics was measured with an oscilloscope to be 0.005 sec. This was independently determined from single-pole model fits to measurements of the system response to square pulses of known duration. The large fixed aperture and the poor observing conditions (intermittent cloudiness and high humidity) resulted in a large sky contribution to the DC observations. Consequently, reliable event times could be determined for only four rings. The square-well profile fit results are given in Table V.

D. The 24 May 1985 Occultation of U25

The occultation of U25 was observed by us from Cerro Tololo, McDonald Observatory, and the IRTF. The event was also recorded at Mt. Palomar, where we had dispatched our fourth clock to insure that all high-quality data sets would be on a common time base. The Mt. Palomar observations will be published separately by the principals involved (P. Nicholson and K. Mathews, private communication). The stellar diameter of U25 adopted for this analysis (Table II) was determined from square-well model fits to narrow ring profiles observed from CTIO and McDonald Observatory. Selected ring profiles of the α, δ, and ε rings are included in Figs. 1, 2, and 3.

TABLE IX

RESULTS OF SQUARE-WELL RING PROFILE FITS TO 26 APRIL 1986 OBSERVATIONS OF U28 FROM IRTF

Ring	Event	Midtime (UTC)	Width (km)	Equivalent width E (km)	Equivalent depth A (km)	Fractional transmission f_0	Normal optical depth	True anomaly (deg)
6	I	13:38:59.456 ± 0.001	1.53 ± 0.08	{0.56 ± 0.01}	{0.70 ± 0.01}	{0.63 ± 0.02}	[0.46]	238.9
6	E	15:00:16.210 ± 0.001	1.66 ± 0.08	{0.55 ± 0.01}	{0.67 ± 0.01}	{0.66 ± 0.02}	[0.40]	130.5
5	I	13:38:24.221 ± 0.001	1.92 ± 0.05	{1.10 ± 0.01}	{1.64 ± 0.03}	{0.42 ± 0.02}	[0.86]	253.0
5	E	15:00:54.313 ± 0.001	1.77 ± 0.04	{1.05 ± 0.01}	{1.61 ± 0.03}	{0.40 ± 0.02}	[0.91]	143.8
4	I	13:37:52.645 ± 0.001	2.56 ± 0.03	{0.91 ± 0.01}	{1.13 ± 0.01}	{0.64 ± 0.01}	[0.44]	181.2
4	E	15:01:17.215 ± 0.003	1.66 ± 0.10	{0.84 ± 0.03}	{1.18 ± 0.05}	{0.49 ± 0.03}	[0.71]	71.4
α	I	13:34:50.183 ± 0.001	6.98 ± 0.02	{3.83 ± 0.02}	{5.59 ± 0.03}	{0.44 ± 0.01}	[0.80]	273.1
α	E	15:04:27.639 ± 0.001	10.32 ± 0.03	{4.64 ± 0.03}	{6.20 ± 0.04}	{0.54 ± 0.01}	[0.60]	159.6
β	I	13:33:27.657 ± 0.001	11.30 + 0.03	{2.94 ± 0.02}	{3.41 ± 0.02}	{0.74 ± 0.01}	[0.30]	177.3
β	E	15:05:44.903 ± 0.001	8.02 ± 0.03	{3.01 ± 0.02}	{3.78 ± 0.03}	{0.62 ± 0.01}	[0.47]	62.2
η	I	13:31:21.111 ± 0.002	2.71 ± 0.06	{0.74 ± 0.01}	{0.87 ± 0.01}	{0.72 ± 0.01}	[0.32]	187.7
η	E	15:07:54.030 ± 0.002	3.30 ± 0.08	{0.75 ± 0.01}	{0.85 ± 0.01}	{0.77 ± 0.01}	[0.26]	70.3
γ	I	13:30:42.779 ± 0.001	2.15 ± 0.03	{1.94 ± 0.01}	{5.18 ± 0.25}	{0.09 ± 0.01}	[2.41]	118.5
γ	E	15:08:31.954 ± 0.001	2.09 ± 0.03	{1.92 ± 0.01}	{5.46 ± 0.32}	{0.07 ± 0.01}	[2.61]	0.4
δ	I	13:29:47.150 ± 0.001	2.77 ± 0.03	{1.94 ± 0.01}	{3.40 ± 0.05}	{0.29 ± 0.01}	[1.23]	24.1
δ	E	15:09:28.091 ± 0.001	3.31 ± 0.01	{2.38 ± 0.01}	{4.25 ± 0.06}	{0.27 ± 0.01}	[1.28]	265.1
ε	E	15:13:46.828 + 0.003	82.47 ± 0.07	{52.90 ± 0.17}	{85.38 ± 0.47}	{0.35 ± 0.01}	[1.04]	133.6

Note. I and E stand for ingress and egress, respectively. Numbers in square brackets were derived from other parameters in the fit. Numbers in braces were derived from separate fits and are alternative representations of the transparency of the ring. See text for discussion of errors.

TABLE X

RESULTS OF SQUARE-WELL RING PROFILE FITS TO 24–25 JANUARY 1986 OBSERVATIONS VOYAGER 2 TIDBINBILLA (X-BAND)

Ring	Event	Midtime (UTC)	Width (km)	Equivalent width E (km)	Equivalent depth A (km)	Fractional transmission f_0	Normal optical depth	True anomaly (deg)
6	I	22:46:41.232 ± 0.002	0.90 ± 0.04	{0.55 ± 0.03}	{0.86 ± 0.06}	{0.38 ± 0.03}	[0.96]	144.3
6	E	1:18:23.434 ± 0.004	1.41 ± 0.06	{0.62 ± 0.03}	{0.83 ± 0.06}	{0.55 ± 0.02}	[0.59]	2.7
5	I	22:45:47.861 ± 0.003	2.62 ± 0.05	{1.31 ± 0.04}	{1.83 ± 0.09}	{0.49 ± 0.02}	[0.70]	150.0
5	E	1:19:06.702 ± 0.002	1.17 ± 0.03	{0.93 ± 0.03}	{1.90 ± 0.11}	{0.19 ± 0.02}	[1.62]	7.9
4	I	22:45:16.749 ± 0.002	1.41 ± 0.04	{0.90 ± 0.03}	{1.45 ± 0.09}	{0.35 ± 0.02}	[1.03]	71.2
4	E	1:19:55.931 ± 0.003	1.86 ± 0.05	{0.93 ± 0.04}	{1.29 ± 0.08}	{0.49 ± 0.02}	[0.70]	288.9
α	I	22:40:48.536 ± 0.005	9.42 ± 0.08	{4.34 ± 0.11}	{5.84 ± 0.21}	{0.53 ± 0.01}	[0.62]	124.4
α	E	1:24:15.860 ± 0.002	3.86 ± 0.04	{3.00 ± 0.06}	{5.90 ± 0.29}	{0.21 ± 0.02}	[1.53]	340.2
β	I	22:38:57.595 ± 0.003	5.07 ± 0.05	{2.70 ± 0.07}	{3.87 ± 0.14}	{0.46 ± 0.01}	[0.76]	13.9
β	E	1:26:15.767 ± 0.005	8.33 ± 0.08	{3.11 ± 0.08}	{3.90 ± 0.13}	{0.62 ± 0.01}	[0.47]	228.9
η	I	22:35:49.531 ± 0.003	1.37 ± 0.05	{0.67 ± 0.03}	{0.92 ± 0.06}	{0.51 ± 0.02}	[0.67]	3.7
η	E	1:29:17.723 ± 0.003	1.10 ± 0.06	{0.53 ± 0.03}	{0.74 ± 0.05}	{0.51 ± 0.03}	[0.67]	217.5
γ	I	22:34:55.037 ± 0.001	3.65 ± 0.02	{3.29 ± 0.04}	{8.74 ± 0.44}	{0.09 ± 0.01}	[2.40]	288.9
γ	E	1:30:12.362 ± 0.001	1.37 ± 0.02	{1.36 ± 0.02}	{13.95 ± 8.12}	{0.00 ± 0.01}	[10.16]	142.4
δ	I	22:33:31.891 ± 0.003	5.18 ± 0.04	{3.24 ± 0.07}	{5.12 ± 0.18}	{0.37 ± 0.01}	[0.99]	186.2
δ	E	1:31:33.195 ± 0.002	2.23 ± 0.04	{1.85 ± 0.05}	{4.05 ± 0.27}	{0.16 ± 0.02}	[1.81]	39.2
ε	I	22:28:26.920 ± 0.002	22.25 ± 0.03	{21.37 ± 0.13}	{78.21 ± 4.52}	{0.03 ± 0.01}	[3.52]	30.0
ε	E	1:37:39.813 ± 0.005	74.86 ± 0.08	{52.30 ± 0.61}	{90.77 ± 2.07}	{0.29 ± 0.01}	[1.21]	241.2

Note. I and E stand for ingress and egress, respectively. All errors are formal errors. Numbers in square brackets were derived from other parameters in the fit. Numbers in braces were derived from separate fits and are alternative representations of the transparency of the ring.

Cerro Tololo. We modified our observing procedure at CTIO from that used for the U23 event in order to observe in the DC mode, using the monitor channel of the infrared spectrometer. Observing conditions were partly cloudy, with good seeing, and sky background levels were determined at several points during the occultation. The results of the profile fits are given in Table VI.

McDonald Observatory. Observations from McDonald Observatory were carried out with the same instrumentation that was used for the U23 occultation, described above. The sky was clear, with high humidity (90%). The background signal strength was stable throughout the occultation. We made an extensive set of measurements of the system time response. Square pulses from a signal generator with widths from 0.05 to 500 msec were fed to an infrared LED, triggered at 1 Hz by the portable clock. The response of the detector to the pulses was recorded at a time resolution of 0.5 msec, along with the triggering time signal. Although the measurements could be approximately matched using a single-pole impulse response function with a time constant of about 0.02 sec, we elected instead to deconvolve the empirically determined impulse response function from the occultation data. We used an FFT (fast Fourier transform) algorithm and the convolution theorem to reconstruct the input signal prior to filtering by the electronics. After deconvolution, all data points were statistically independent (uncorrelated), as assumed by the least-squares algorithm used for the square-well profile fits. The results of the profile fits are given in Table VII.

IRTF. Observations at the IRTF on Mauna Kea were carried out with the infrared photometer under very poor conditions, with increasing cloudiness as the occultation approached. Only the ε-ring egress profile could be detected with certainty, and because of the strongly varying background signal, the signal from the occultation star itself could not be calibrated. Consequently, we were able to fit only for the ring midtime and width, as shown in

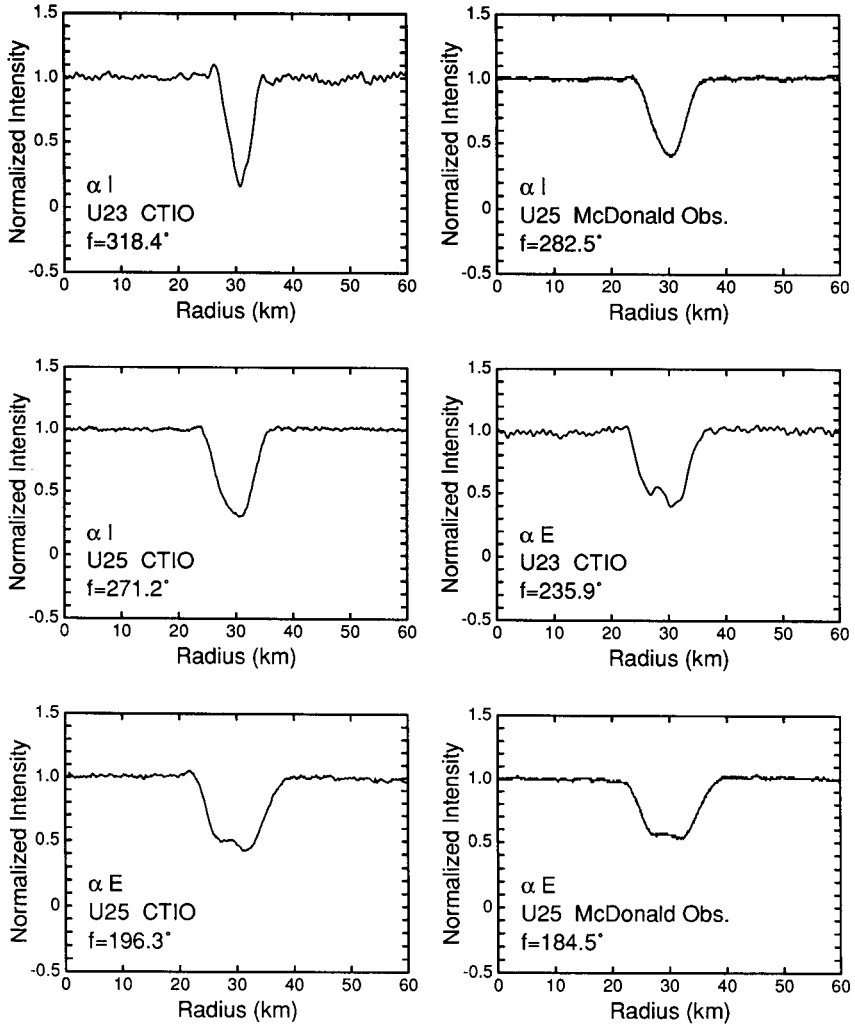

FIG. 1. Selected occultation ring profiles of the α ring obtained during May 1985. The occultation star, observatory, event (I for ingress, E for egress), and true anomaly, f, are indicated for each profile.

Table VIII. The GRABBER program was used for data recording.

E. The 26 April 1986 Occultation of U28

This occultation was successfully observed using the IRTF on Mauna Kea. (Observations were also made by D. Tholen at the University of Hawaii 2.24-m telescope at a wavelength of 8600 Å, but these data have low S/N and are not included in the present analysis.) Observing conditions were excellent throughout the event, and the background was quite steady. Nevertheless, several "false" events were present in the lightcurve which had similar depths to the known rings. Later observations of the field showed an infrared source about 5 arcsec away from the occultation star. The false events were most likely due to seeing fluctuations or guiding problems causing this star to drift in and out of the 10 arcsec aperture. The brightness of the star is consistent with this interpretation.

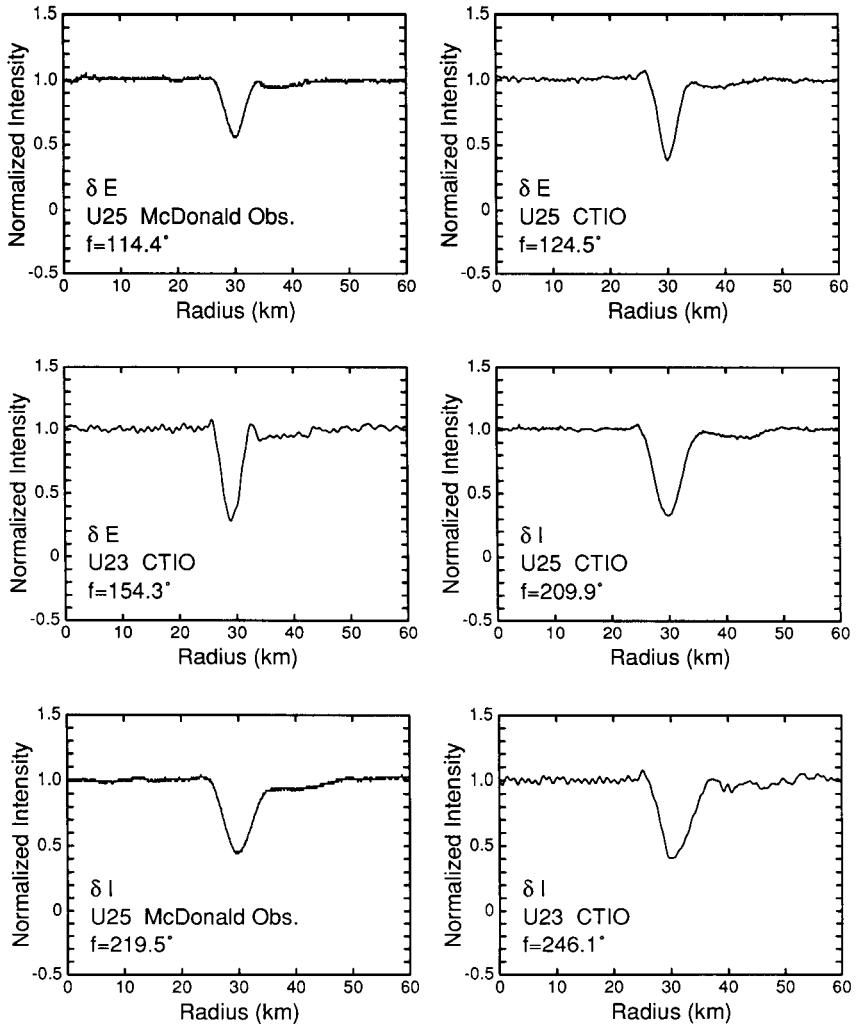

FIG. 2. Selected occultation ring profiles of the δ ring obtained during May 1985. The occultation star, observatory, event (I for ingress, E for egress), and true anomaly, f, are indicated for each profile.

The instrumental response function was measured by slewing the telescope rapidly across a star. A satisfactory fit was obtained by modeling the system response as a single-pole filter with a time constant of 0.05 sec. The stellar diameter for this occultation was unusually small and was determined from fits to the sharpest-edged narrow rings, 6, 4, η, and γ. (It is evident from the data that the edges of several rings are not sharp, and using a square-well model to fit for the stellar diameter with such profiles would have resulted in an erroneously large value.)

All nine of the major rings were observed on both ingress and egress, with the exception of the ε ingress occultation, which unfortunately occurred while the star was being recentered in the aperture. High S/N immersion and emersion atmospheric occultations were also recorded; these will be presented elsewhere. The individual ring profiles are shown in Figs. 4 and 5, along with the best-fitting diffracted square-well

model profiles. The asymmetry of the profiles reflects the influence of the finite response time of the detector. The models fit remarkably well for most of the rings, but there are clear deviations for the α and β rings. Faint ring material is present near the outer edge of the η ring and the inner edge of the δ ring. The apparent structure near the inner edge of ring 4 egress profile is probably due to the companion star drifting out of the aperture, as described above. The ε-ring profile shows much structure, with the resolution being limited primarily by diffraction, not by the finite diameter of the star. Table IX contains the results of the profile fits.

III. VOYAGER RING OCCULTATION OBSERVATIONS AND DATA ANALYSIS

Voyager occultation data provide strong constraints on the ring orbital elements and the direction of the planetary pole. This is primarily because of the different viewing geometry for Earth-based and spacecraft occultations. Currently, Uranus is nearly pole-on to the Earth, making it difficult to

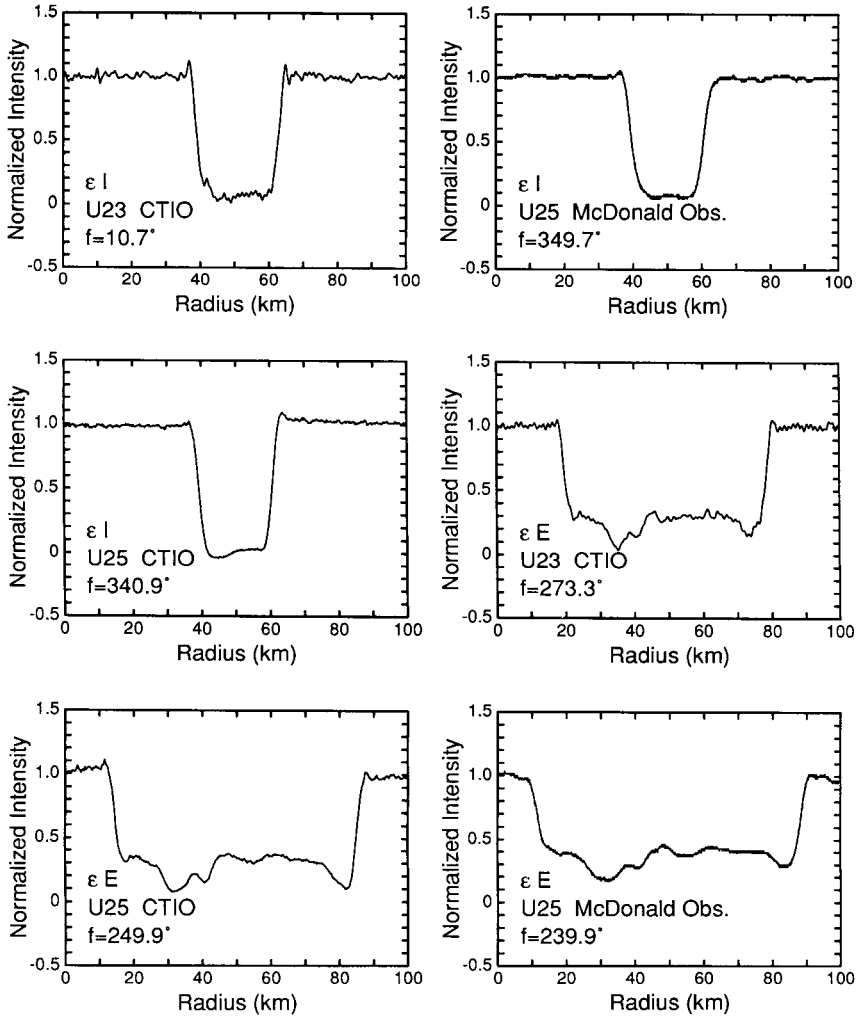

FIG. 3. Selected occultation ring profiles of the ε ring obtained during May 1985. The occultation star, observatory, event (I for ingress, E for egress), and true anomaly, f, are indicated for each profile.

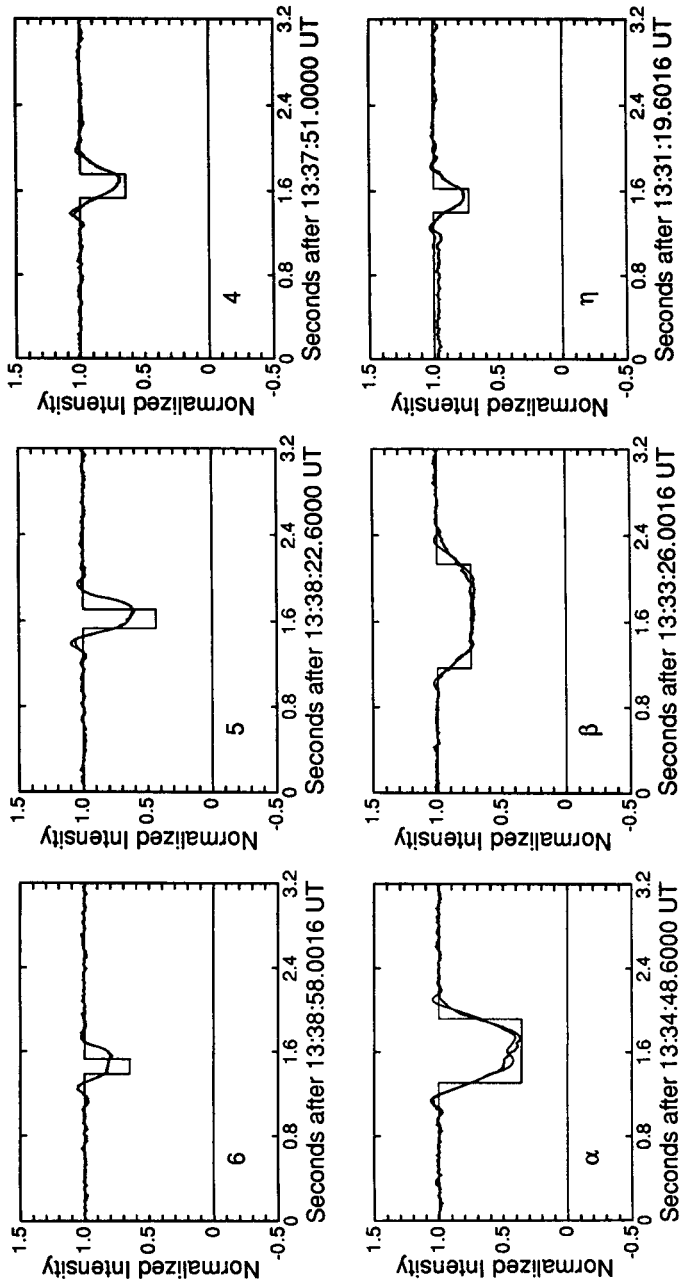

FIG. 4. Square-well model fits to ingress ring profiles obtained from the IRTF of the 26 April 1986 occultation of U28. The data are plotted at 0.0032 sec per point. Superimposed on each profile is the best-fitting diffracted square-well model. The ε ring profile was not observed because the star was being recentered in the aperture at the time.

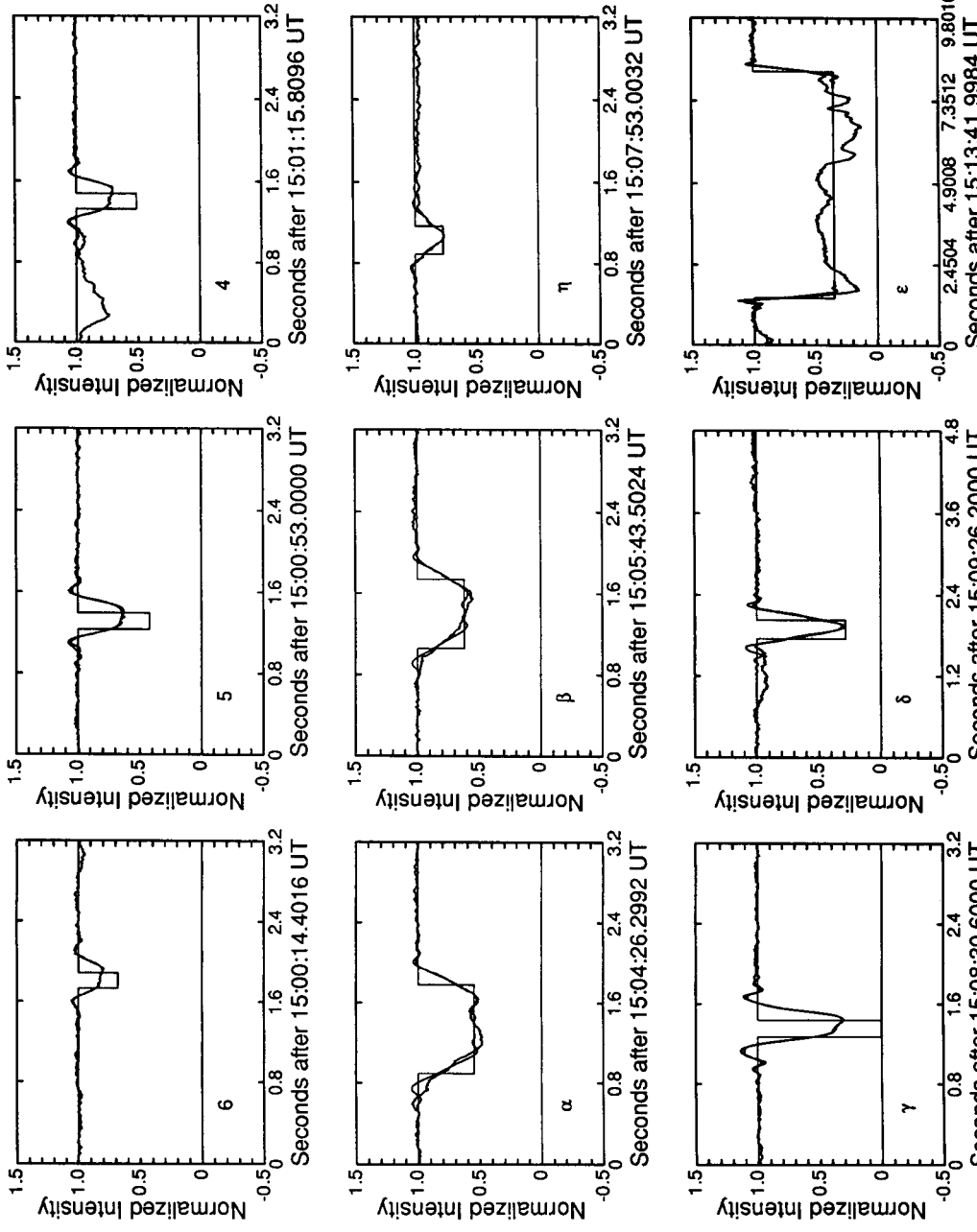

FIG. 5. Square-well model fits to egress ring profiles obtained from the IRTF of the 26 April 1986 occultation of U28. The data are plotted at 0.0032 sec per point. Superimposed on each profile is the best-fitting diffracted square-well model. The apparent structure adjacent to ring 4 is probably due to a seeing fluctuation; see the text for details.

improve the determination of the ring inclinations through Earth-based observations alone. Determination of the absolute radius scale of the rings from Earth-based data alone is hindered by the large a priori uncertainty in the relative locations of the planet and the occulted stars, which must be included as free parameters in the fit. Voyager occultations occurred both pole-on (radio occultations) and at oblique incidence (σ Sgr and β Per occultations). Since the spacecraft location relative to Uranus is known to an accuracy of about 1 km, the radio results provide a very accurate determination of the absolute radius scale of the ring system. The σ Sgr and β Per data are strong constraints on the planetary pole and ring inclinations.

A. Radio Science Occultations

All nine main rings were observed on both ingress and egress by the Voyager radio science experiment. Data were recorded using the Deep Space Station at Tidbinbilla and the Australian National Radio Astronomy Observatory at Parkes, at both S- and X-band, but we restrict our attention here to the X-band (3.6 cm) Tidbinbilla data. We fitted the observed ring profiles using a square-well point-source diffraction model, with the results shown in Figs. 6 and 7 and tabulated in Table X. The square-well model gives a remarkably good fit to several events (particularly the γ-ring egress profile), although results from Fresnel deconvolution of the data show considerable radial structure in all of the rings (L. Tyler and E. Marouf, private communication).

B. Voyager Stellar Occultations

Two stellar occultations by the rings were observed with the Voyager 2 spacecraft: the high S/N σ Sgr occultation whose chord passed just interior to the δ ring, and the lower S/N β Per occultation by the complete ring system. These occultations were observed simultaneously by the UVS at $\approx$1100 Å and the PPS at 2650 Å. Inclinations of the line of sight to the mean ring plane were about 62.9° for σ Sgr and $-53.2°$ for β Per, which was observed from the anti-Sunward side of the rings. The proximity of the spacecraft to the rings yielded high-resolution ring profiles virtually unaffected by diffraction. The resulting ring profiles are discussed in detail by Holberg *et al.* (1987) and Lane *et al.* (1986), for the UVS and PPS, respectively.

The UVS times are taken from Holberg *et al.* (1987), and L. Esposito, A. L. Lane, and L. Horn kindly provided estimates of ring midtimes from the PPS occultation observations. Upon comparison of the UVS and PPS midtimes for the same events, it became evident that there was a systematic offset of more than 1 sec between the two data sets. From trial ring orbit solutions using both Earth-based and Voyager data, we found that the PPS times gave a much poorer fit than the UVS times, and we determined that the two data sets could best be brought into accord by adding 1.18 sec to the nominal PPS times. Subsequent investigation of the Voyager software has confirmed that an offset of between 1.18 and 1.20 sec should be added to nominal PPS times (L. Esposito, A. L. Lane, and R. West, private communication), although the precise value has yet to be determined. For this analysis, we have adopted an offset of exactly 1.18 sec. The midtimes used for the present analysis are summarized in Tables XI and XII, where the times are specified as the UTC of the ring events *as observed on the spacecraft.*

TABLE XI

ADOPTED RING EVENT TIMES AT VOYAGER 2 σ SGR OCCULTATION 24 JANUARY 1986

Ring	Event	PPS (UTC)	UVS (UTC)
δ	Ingress	6:16:04.23	6:16:04.25 ± 0.27
δ	Egress	7:21:37.78	7:21:37.31 ± 0.27
1986U1R	Ingress	5:30:42.30	5:30:42.48 ± 0.15
1986U1R	Egress	8:06:57.19	8:06:57.50 ± 0.05
ε	Ingress	5:15:53.82	5:15:54.03 ± 0.03
ε	Egress	8:19:47.595	8:19:47.65 ± 0.03

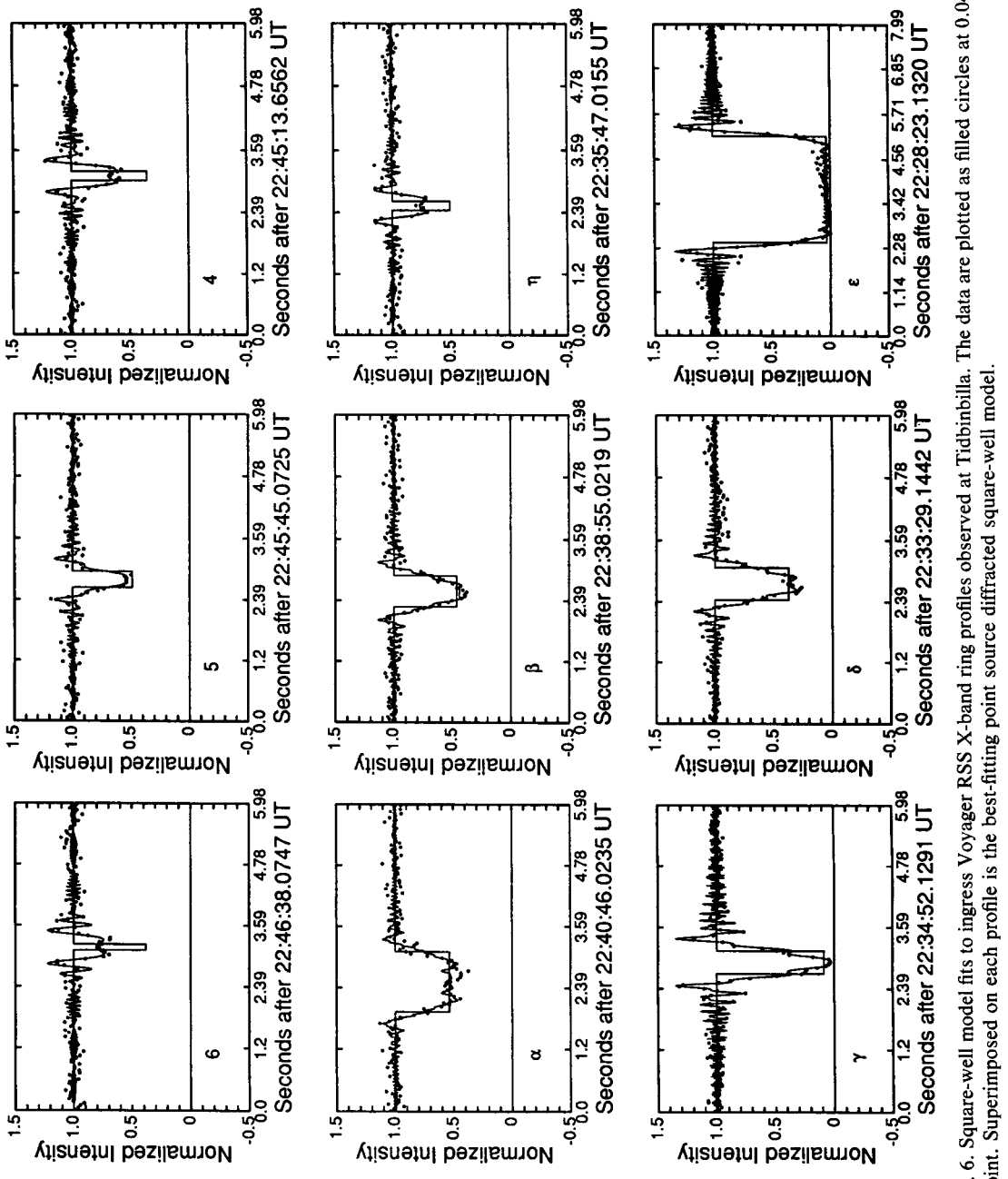

FIG. 6. Square-well model fits to ingress Voyager RSS X-band ring profiles observed at Tidbinbilla. The data are plotted as filled circles at 0.04096 sec per point. Superimposed on each profile is the best-fitting point source diffracted square-well model.

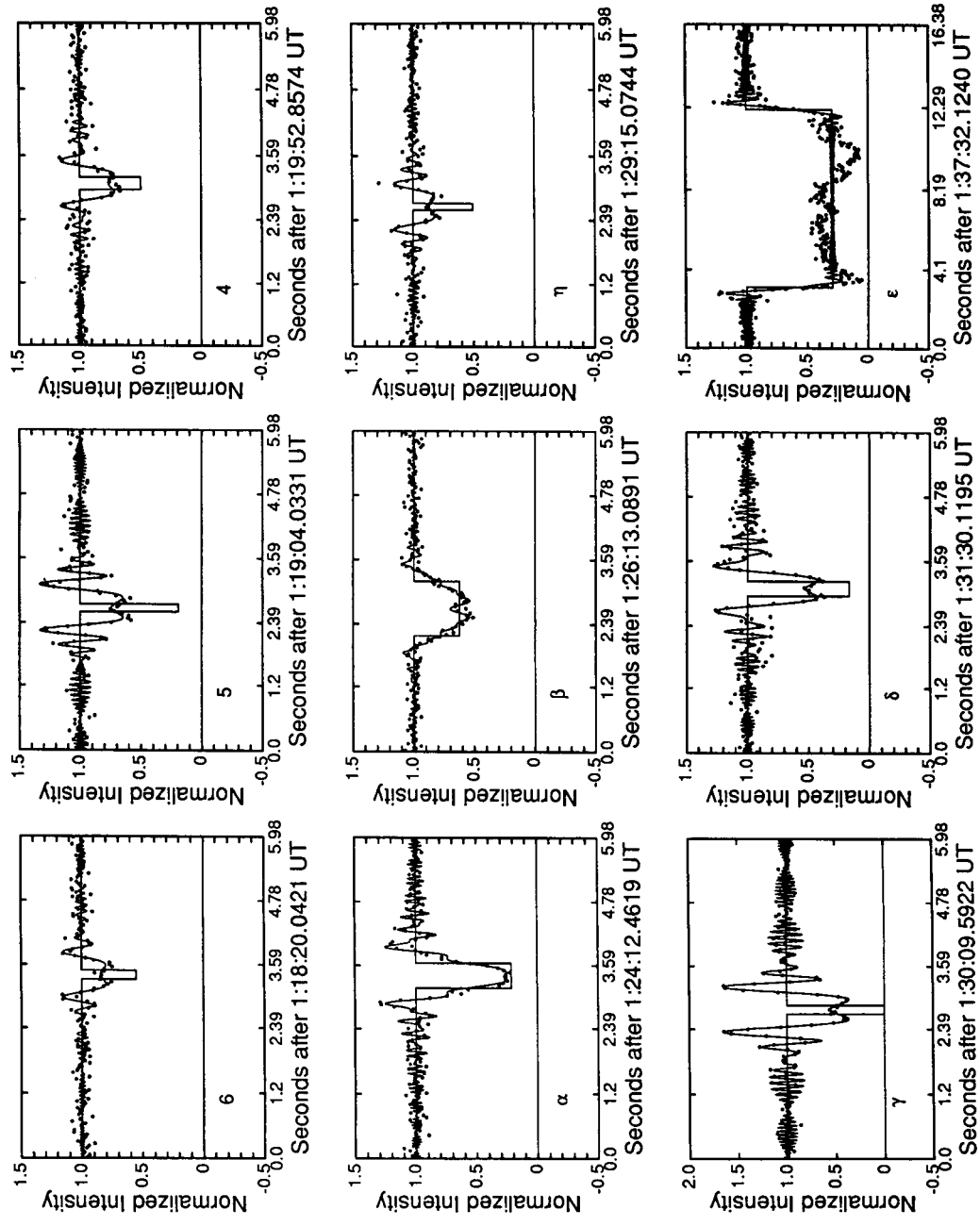

FIG. 7. Square-well model to egress Voyager RSS X-band ring profiles observed at Tidbinbilla. The data are plotted as filled circles at 0.04096 sec per point. Superimposed on each profile is the best-fitting point source diffracted square-well model.

TABLE XII

ADOPTED RING EVENT TIMES AT VOYAGER 2 β PER OCCULTATION 24 JANUARY 1986

Ring	Event	PPS (UTC)	UVS (UTC)
6	Egress	19:28:28.55	
5	Ingress	18:42:44.18	
5	Egress	19:29:10.98	
4	Ingress	18:42:14.80	
4	Egress	19:29:49.19	
α	Ingress	18:38:44.56	
α	Egress	19:33:16.66	
β	Ingress	18:37:21.53	
β	Egress	19:34:43.10	
η	Egress	19:36:55.67	
γ	Ingress	18:34:26.56	
γ	Egress	19:37:34.41	
δ	Ingress	18:33:28.76	
δ	Egress	19:38:31.78	
ε	Ingress	18:29:46.325	
ε	Egress	19:42:56.72	19:42:56.85 ± 0.14

IV. ORBIT DETERMINATION

A. General Considerations

Our goal is to determine the Uranus ring system geometry and orbital elements by constructing a model for the planet and rings that best matches the observed set of ring occultation event midtimes. The free parameters in the least-squares fit to the midtimes include the direction of the planetary pole, the gravitational harmonic coefficients J_2 and J_4, the Keplerian orbital elements of the rings, corrections to the predicted relative locations of the occultation stars and the planet, and offsets to the time base used at a given observatory.

Our method is as described by French *et al.* (1986a) with the following exceptions:

- Voyager data have been accommodated, as described in more detail below.
- The "reference time" for ring elements is now defined as 20:00 UT on 10 March 1977 *at Uranus*, rather than at the Earth.
- Ring longitudes are now measured in a prograde direction from the ascending node of Uranus' equator on the Earth's equator of 1950.0, rather than on the Earth's equator at the reference time. The two systems are related as follows: longitude (new) = longitude (old) + 0.153°.
- A revised value for GM of Uranus has been used: GM = 5.793939×10^{21} cm^3 g^{-1} sec^{-2} (Tyler *et al.* 1986).
- The least-squares fit now (optionally) minimizes the sum of squared residuals in ring radius, rather than in ring event time. This is preferable when, as in the present case, there is a wide range of event velocities and the post-fit residuals frequently greatly exceed the formal uncertainties in the midtimes of several of the rings.

B. Spacecraft Occultation Geometry

To incorporate the Voyager occultation data in the orbit model, we compared the observed occultation midtimes to the predicted times based on the assumed ring orbital elements, the spacecraft trajectory, the positions of the occultation stars (for the stellar occultations), and the location of the Earth-based tracking station (for radio occultations). The calculations were performed in a heliocentric reference frame to simplify the treatment of aberrations, and light travel time is taken into account as necessary. No corrections were made for the gravitational deflection of light; these are entirely negligible since the spacecraft was so near to Uranus during the occultations.

We used the trajectory information provided by the Navigation Team (R. Cesarone, personal communication), based on PFILE tape K2742, file 3, NAV ID T860502. The planetocentric spacecraft position was tabulated every minute for the occultation periods, and a fourth-order Bessel interpolation scheme was used to determine the spacecraft position for any desired time. For the radio occultation analysis, we used the JPL DE-125 ephemeris, provided by M. Standish (personal communication), to determine the heliocentric coordinates of the Earth and Uranus.

The catalog positions of σ Sgr and β Per were corrected for proper motion and par-

TABLE XIII

VOYAGER OCCULTATION STARS

σ Sgr		
Coordinate frame	α (1950.0)	δ (1950.0)
FK4 (1950.0)	$18^h52^m09.9270^s$	$-26°21'38.290''$
Heliocentric, no parallax	$18^h52^m09.9645^s$	$-26°21'40.234''$
Heliocentric, parallax	$18^h52^m09.9731^s$	$-26°21'40.239''$
Spacecraft-centered, aberration	$18^h52^m10.1458^s$	$-26°21'39.618''$
Proper motion (1950–1986)	$+0.0375^s$	$-1.944''$
Parallax correction	$+0.0086^s$	$-0.005''$

Ring plane radius partial derivatives

Ring	Event	$\frac{\partial r}{\partial \alpha}$ (km/sec)	$\frac{\partial r}{\partial \delta}$ (km/″)
ε	Ingress	+14	−3.5
δ	Ingress	+2	−3.3
δ	Egress	−10	−2.9
ε	Egress	−16	−2.4

β Per		
Coordinate frame	α (1950.0)	δ (1950.0)
FK4 (1950.0)	$3^h04^m54.3560^s$	$+40°45'52.460''$
Heliocentric, no parallax	$3^h04^m54.3672^s$	$+40°45'52.547''$
Heliocentric, parallax	$3^h04^m54.3919^s$	$+40°45'52.416''$
Spacecraft-centered, aberration	$3^h04^m53.1491^s$	$+40°45'50.573''$
Proper motion (1950–1986)	$+0.0112^s$	$-0.087''$
Parallax correction	$+0.0247^s$	$-0.130''$

Ring plane radius partial derivatives

Ring	Event	$\frac{\partial r}{\partial \alpha}$ (km/sec)	$\frac{\partial r}{\partial \delta}$ (km/″)
ε	Ingress	+4	+0.2
β	Ingress	+4	+0.3
6	Ingress	+3	+0.3
6	Egress	−6	+0.8
β	Egress	−7	+0.7
ε	Egress	−8	+0.7

allax before being used for ring geometry solutions. The successive corrections are summarized in Table XIII. We began with the FK4 (1950.0) catalog position and then computed the heliocentric EME50 position of the star at the occultation epoch by applying proper motion corrections (radial velocity of the star is ignored). The new positions are listed as "heliocentric, no parallax" in the table. Next, we applied a parallax correction appropriate for the spacecraft position with respect to the Sun and each star. These positions are listed as "heliocentric, parallax" in the table, and are appropriate for orbit model calculations performed in a heliocentric rest frame, as was done for this paper. For completeness, we determined the spacecraft-centered stellar coordinates by applying the aberration due to heliocentric motion of the spacecraft. The new position is listed as "spacecraft-centered, aberration." When this position is used for calculations, it must be remembered that the aberration correction includes the sum of the aberration due to the motion of Uranus with respect to the Sun and the aberration due to the motion of the spacecraft relative to Uranus. When using a *planet-centered* reference frame for orbit calculations, it is necessary to account properly for the planetary component of the aberration.

We determined the effect of a star position error on derived ring plane radii as follows:

(1) The "heliocentric, parallax" stellar positions and the ring orbital elements and pole direction of French *et al.* (1986a) were used to determine the ring plane radii corresponding to the times of representative ring occultations for both the σ Sgr and the β Per occultations (Tables XI and XII).

(2) The right ascension of each star was changed by $+0.01^s$, and new ring plane radii were computed. The resulting change was used to calculate the derivative $\partial r/\partial \alpha$ in Table XIII.

(3) The declination of each star was changed by $+0.001''$, and new ring plane radii were computed. The resulting change was used to calculate the derivative $\partial r/\partial \delta$ in Table XIII.

The results show that ring plane radii are more sensitive to errors in the position of σ Sgr than the position of β Per, but even in the worst case, a position error as large as $0.1''$ would still lead to errors in ring plane radii of only a few hundred meters. The mean errors in the FK4 positions in right ascension and declination are given as (0.0019^s, $0.027''$) for σ Sgr and (0.0016^s, $0.024''$) for β Per, corresponding to errors in ring plane radii of less than 100 m. Another source of error is the possible systematic differences between the FK4 reference system and the coordinate system used by JPL for the spacecraft trajectory, estimated to be of order $0.1''$.

We tested our implementation of the spacecraft occultation geometry by comparing representative calculations with independent predictions by P. Rosen and D. Gresh (personal communication) for radio occultation events and by P. Nicholson (personal communication) for stellar occultations. In all cases, the agreement was good to ±1 m in ring-plane radius.

C. Eccentric Ring Orbit Solution

We used the new Earth-based occultation data (Tables III–IX) and the Voyager occultation results (Tables X–XII), along with all previous Earth-based data (French *et al.* 1986a) in a least-squares solution for the orbits of the rings. Previous ring orbit solutions have shown that the γ and δ rings cannot be well-matched with elliptical orbits. Therefore, we determined the best-fitting eccentric ring orbital elements in two steps. First, we fitted for the planetary pole, J_2, J_4 corrections to the Earth-based occultation star positions, time offsets for selected stations, and the orbital elements for all rings *except* γ, δ, and 1986U1R. Second, we fitted for the orbital elements of these three rings, with all other parameters fixed at the values determined from the first fit. (Because 1986U1R was detected only in the σ Sgr occultation data, it was fitted to an equatorial, circular orbit model.) The results of these two fits are given in Table XIV. The upper panel of Fig. 8 shows the ring-plane residuals from the best-fitting eccentric ring orbits for all of the rings.

The *formal* errors in most of the fitted parameters are remarkably small. For example, the formal error in the ring 6 semimajor axis is only 0.15 km. This is clearly

TABLE XIV

URANUS ECCENTRIC RING ORBIT SOLUTION FROM EARTH-BASED AND VOYAGER 2 OCCULTATION OBSERVATIONS

Ring	Eccentric ring orbital elements[a]					
	Semimajor axis a (km)	Eccentricity e (× 10^3)	Longitude of periapse $\tilde{\omega}_0$ (deg)[b]	Inclination i (deg)	Longitude of ascending node Ω_0 (deg)[b]	RMS ring orbit residual (km)
6	41837.15 ± 0.26	1.013 ± 0.004	242.80 ± 0.34	0.0616 ± 0.0010	12.12 ± 0.62	0.32
5	42234.82 ± 0.27	1.899 ± 0.005	170.31 ± 0.29	0.0536 ± 0.0013	286.57 ± 0.74	0.27
4	42570.91 ± 0.28	1.059 ± 0.004	127.28 ± 0.29	0.0323 ± 0.0006	89.26 ± 1.70	0.27
α	44718.45 ± 0.22	0.761 ± 0.004	333.24 ± 0.27	0.0152 ± 0.0006	63.08 ± 2.92	0.32
β	45661.03 ± 0.13	0.442 ± 0.003	224.88 ± 0.56	0.0051 ± 0.0006	310.05 ± 11.50	0.26
η	47175.91 ± 0.14	(0.004 ± 0.003)	(228.1 ± 57.7)	(0.0011 ± 0.0008)	(188.73 ± 30.81)	0.49
γ[c]	*47627.16 ± 0.66*	*(0.099 ± 0.017)*	*(137.3 ± 12.2)*	*(0.0059 ± 0.0041)*	*(142.2 ± 42.9)*	*3.35*
δ[c]	*48299.33 ± 0.65*	*(0.038 ± 0.017)*	*(152.9 ± 26.1)*	*(0.0019 ± 0.0038)*	*(223.2 ± 111.5)*	*2.05*
1986 U1R	50023.94 ± 0.34	(0.0)	(0.0)	(0.0)	(0.0)	0.51
ε	51149.32 ± 0.13	7.936 ± 0.005	214.97 ± 0.06	(0.0002 ± 0.0008)	(246.6 ± 155.2)	0.60

Harmonic coefficients of the gravity potential[d]

$J_2 = (3.34343 \pm 0.00032) \times 10^{-3}$
$J_4 = (-2.885 \pm 0.045) \times 10^{-5}$

Pole of the equatorial plane (deg)

α (1950.0) 76.5969 ± 0.0034
δ (1950.0) 15.1117 ± 0.00033

Fitted time offsets

Date	Station	Offset (sec)
15 Aug. 1980	ESO	0.051 ± 0.028
22 Apr. 1982	ESO	−0.147 ± 0.011
22 Apr. 1982	LCO	−0.032 ± 0.010
22 Apr. 1982	Tenerife I	−0.116 ± 0.027
22 Apr. 1982	Tenerife E	0.395 ± 0.032
24 Jan. 1986	PPS	1.18

[a] For GM = 5.793939 × 10^{21} cm^3 g^{-1} sec^{-2}. See text for discussion of quoted errors in all fitted quantities.
[b] At 20:00 UT on 10 March 1977 at Uranus. Longitudes are measured in the prograde direction from the ascending node of Uranus' equator on the Earth's equator of 1950.0.
[c] γ and δ rings were fitted separately. See text for details. *The preferred solutions for these rings include normal modes and are given in Table XV.*
[d] For a reference radius R = 26,200 km.

an underestimate of the true uncertainty, since no account has been taken of possible errors in the spacecraft trajectory, which is uncertain at the 1-km level, according to the Voyager Navigation Team. We performed a separate set of orbit fits to determine the effect of a trajectory error on the derived model parameters. We used the full Earth-based data set, as before, and modified the Voyager data by incrementing the observed ring event times by 0.1 sec, corresponding roughly to an along-track error in the spacecraft position of just over 1 km, at the velocities appropriate for the occultation events. The error bars in Table XIV are the larger of the formal error of the original fit and the difference between the best-fitting values from the two sets of fits. For the example cited above, the difference in the semimajor axis of the ring 6 given by these two fits was 0.26 km, which is the error quoted in Table XIV.

These results represent a considerable improvement on our most recent published orbit model (French *et al.* 1986a). The enhanced Earth-based data set and the Voyager observations have made it possible to pursue a troubling inconsistency between observations of the 22 April 1982 occultation of KME14 from Tenerife and l'Observatoire de Pic du Midi et de Toulouse (OPMT). According to the new solution, the ring event times given by Millis *et al.* (1987) for the Tenerife data must be corrected by the offsets shown in Table XIV. Although we cannot identify the source of the timing error, the corrections are statistically significant and bring all ground-based and Voyager data into consonance. The differences between Table XI of French *et al.*(1986a) and Table XIV can be traced in large part to the new timing offsets applied to the 22 April 1982 Tenerife data. The other timing offsets in Table XI were fitted in order to eliminate possible systematic errors in event timing during occultations observed from more than one station.

V. NORMAL MODES OF THE δ AND γ RINGS

The δ and γ rings deviate significantly from simple precessing ellipses, indicating that important dynamical effects have not been accounted for in the eccentric ring models for these two rings. French *et al.* (1986b) investigated a number of possible perturbations and found that the δ ring could be well matched by a wavenumber $m = 2$ Lindblad resonance with a pattern speed of 23.4383 ± 0.0001 deg hr^{-1}. They attributed this resonance to an unseen small satellite, rather than to a normal mode of the ring, because the observed pattern speed did not appear to match the expected value for a normal mode. No such satellite was found, although it would have been clearly visible in Voyager images. However, the Voyager encounter also yielded a substantially improved value for the planetary mass (Tyler *et al.* 1986), and the value of Standish and Campbell (1984), used by French *et al.* (1986b) in their analysis, was found to be in error by six times its stated error. Since the predicted pattern speed for a given radius depends on the planetary mass, this renewed the possibility that the observed pattern was due to an excited normal mode after all. Porco and Goldreich (1987) found that a slight change in the radius scale of the rings, deduced from expected resonant associations with two shepherd satellites, was consistent with an $m = 2$ internal mode in the δ ring. It remained to be demonstrated, however, that the proposed radius scale change was consistent with the large set of occultation observations.

We have fitted the complete set of observations, including the U28 and Voyager occultations, to a model for the δ ring as the linear sum of an inclined, precessing ellipse (equivalent to an $m = 1$ mode) and an $m = 2$ radial distortion, in the same way as French *et al.* (1986b). The results are given in Table XV, and the data points and the model are shown graphically in Fig. 9. The new data fit the pattern well, and 22 April 1982 observations that had troubled French *et al.* (1986b) were found to have been brought into line with the time offsets discussed above. In fact, the residuals from the reso-

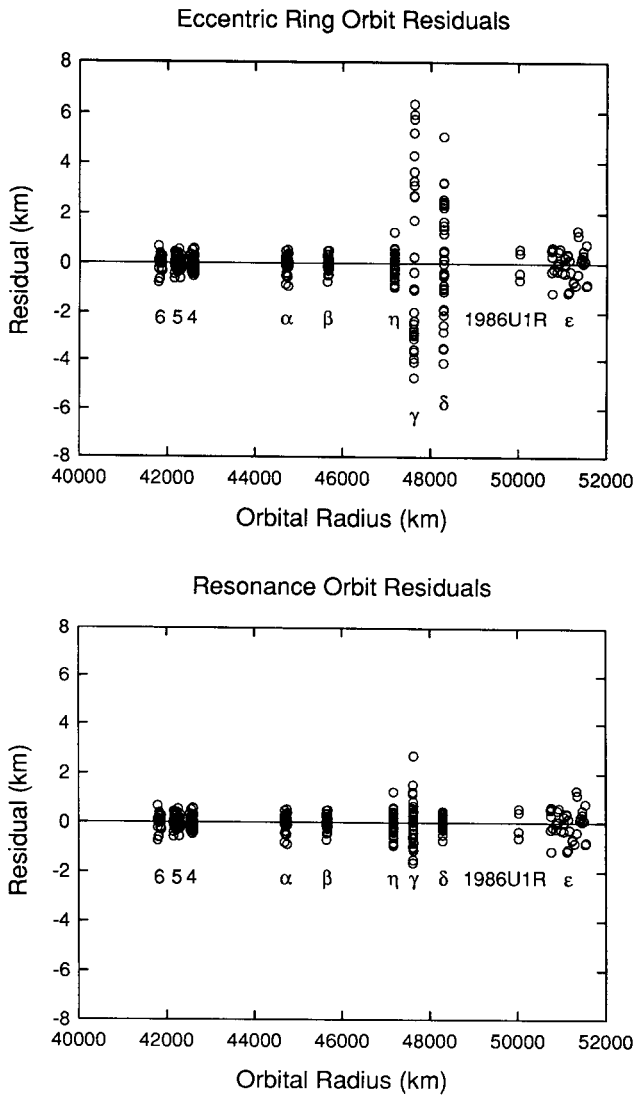

FIG. 8. Orbit model residuals. The upper panel shows the ring-plane radius residuals of the best-fitting precessing, inclined elliptical ring model for each ring. Note the large residuals for the γ and δ rings. When the $m = 0$ normal mode is fitted to the γ ring and the $m = 2$ normal mode is fitted to the δ ring, the residuals for these two rings are substantially reduced, as shown in the lower panel.

nance fit to the δ ring are comparable to the residuals from elliptical fits to the other "well behaved" rings, as shown in the lower panel of Fig. 8. The data can be fitted nearly as well with an $m = 2$ mode alone, as can be seen from the weak statistical significance of the $m = 1$ orbital elements for the δ-ring fit (Table XV).

The fitted semimajor axis for the δ ring is 48300.12 $\pm$ 0.08 km. The expected radial location of an $m = 2$ distortion traveling with the observed pattern speed of 23.43821 $\pm$ 0.00004 deg hr^{-1} is $a_{res} = 48300.19 \pm 0.09$ km. The excellent agreement between these two radii confirms that the distortion in the δ ring is associated with a normal mode, excited either by internal viscous overstabilities (Borderies *et al.* 1985) or by parametric excitation by shepherd satellites (Goldreich and Tremaine 1981).

TABLE XV

NORMAL MODES OF THE γ AND δ RINGS

Parameter	γ ring	δ ring
Wavenumber m	1	1
Semimajor axis a (km)	47626.87 ± 0.28	48300.12 ± 0.08
Eccentricity e ($\times 10^3$)	0.109 ± 0.007	0.004 ± 0.002
Longitude of periapse $\tilde{\omega}_0$ (deg)	132.1 ± 4.3	216.7 ± 29.3
Inclination i (deg)	(0.0015 ± 0.0018)	0.0011 ± 0.0004
Longitude of ascending node Ω_0 (deg)	(251.3 ± 84.8)	260.7 ± 39.0
Wavenumber m	0	2
Amplitude (km)	5.15 ± 0.33	3.11 ± 0.09
Phase ϕ_0 (deg)	302.7 ± 11.7	103.6 ± 2.5
Frequency (deg hr^{-1})	47.73198 ± 0.00019	23.43821 ± 0.00004
Period (hr)	7.54211 ± 0.00003	15.35953 ± 0.00003
Resonance radius a_{res} (km)	47626.24 ± 0.14	48300.19 ± 0.09
$a - a_{res}$ (km)	+0.63	−0.07
RMS ring orbit residual (km)	0.99	0.31

Note. Longitudes and phases correspond to a reference time of 20:00 UT on 10 March 1977 at Uranus. Longitudes are measured in the prograde direction from the ascending node of Uranus' equator on the Earth's equator of 1950.0. GM = 5.793939×10^{21} cm^3 g^{-1} sec^{-2}. See text for discussion of errors in all fitted quantities.

Elliptical orbit fits to the γ ring are even less successful than such fits to the δ ring, with typical ring plane residuals of about 3.5 km (Fig. 8, top panel). French *et al.* (1986b) searched for low wavenumber radial distortions in the data, but none were

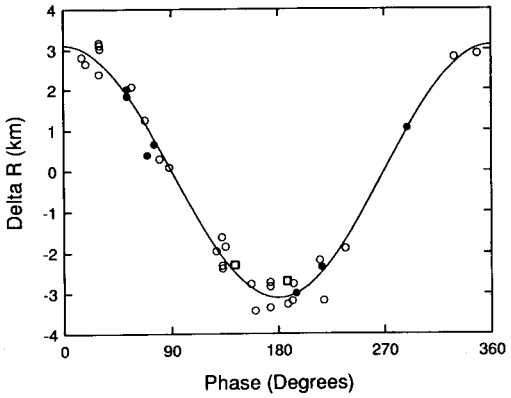

FIG. 9. The best-fitting $m = 2$ mode resonance to the δ ring, as a function of orbital phase. The data points are the observed radius residuals from a circular, equatorial ring orbit. The open circles represent Earth-based occultation data through 1985. The open squares are data from the 26 April 1986 occultation of U28, and the filled circles are Voyager observations.

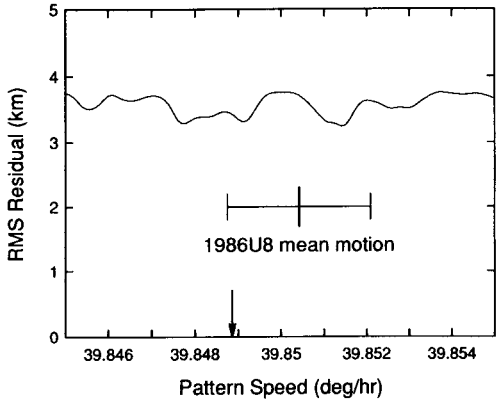

FIG. 10. RMS ring plane residuals as a funtion of pattern speed for the γ ring. For a given pattern speed, the ring was modeled as a combination of an inclined, precessing ellipse (corresponding to an $m = 1$ mode) and an $m = 6$ mode. The pattern speed corresponding to the observed radius of the γ ring, 47626.87 km, is marked with an arrow. This is very close to the 6:5 IER location of 1986U8, shown as a vertical line with an error bar computed from the uncertainty in the orbital period of the satellite. In spite of the proximity of the γ ring to this resonance, its radial orbital variations cannot be due *primarily* to the 6:5 resonance.

found. The discovery by Voyager of a host of small satellites in the vicinity of the rings has prompted us to extend the resonance search. Porco and Goldreich (1987) surveyed the resonances of the known satellites and pointed out that the 6:5 inner eccentric resonance (IER) of 1986U8 falls within a few kilometers of the mean radius of the γ ring. We fitted an $m = 6$ pattern of the γ ring in exactly the same fashion as for the $m = 2$ fits to the δ ring, for a range of pattern speeds. The results of the scan are shown in Fig. 10, which plots the RMS ring plane residual from each fit as a function of the pattern speed assumed for the fit. None of the fits reduced the residuals significantly from the elliptical ring value. The arrow in the figure marks the pattern speed corresponding to the best fitting γ-ring radius, and the mean motion of 1986U8 is also shown, along with its uncertainty, as given by Porco and Goldreich (1987). We conclude that the radial perturbations of the γ ring are not due principally to the 6:5 IER of 1986U8.

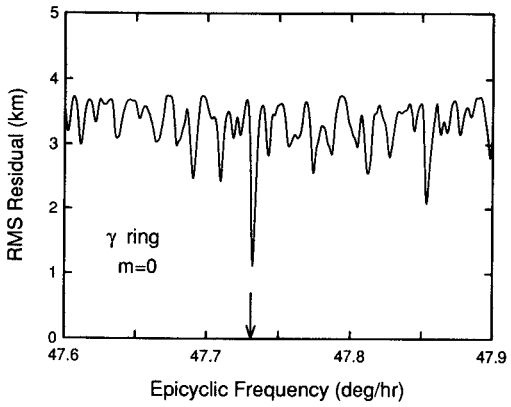

FIG. 11. RMS ring plane residuals as a function of epicyclic frequency for the γ ring. For a given epicyclic frequency, the ring was modeled as a combination of an inclined, precessing ellipse (corresponding to an $m = 1$ mode) and an $m = 0$ mode. There is a sharp mimimum at an epicyclic frequency of 47.73192 deg hr^{-1} (marked by the arrow). The calculated orbital radius of a ring particle with this epicyclic frequency is within 1 km of the fitted orbital radius of the ring. This close agreement is strong evidence that the γ ring is undergoing radial oscillations.

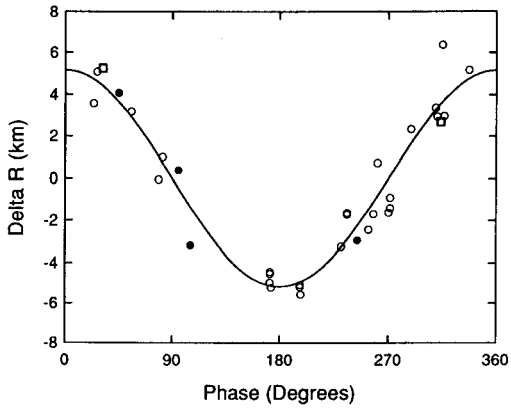

FIG. 12. The best fitting $m = 0$ mode resonance to the γ ring, as a function of the phase of the radial oscillation. The data points are the observed ring-plane radius residuals from an inclined, precessing elliptical orbit ($m = 1$ mode). The open circles represent Earth-based occultation data through 1985. The open squares are data from the 26 April 1986 occultation of U28, and the filled circles are Voyager observations.

We ran a similar series of fits with all other wavenumbers m from 2 to 10, over a range of pattern speeds (both prograde and retrograde) appropriate for the γ ring. None of these fits gave a good match to the data. However, there remained the possibility that the ring might be undergoing radial oscillations (the $m = 0$ mode). This had been investigated by French *et al.* (1986b), but it was dismissed because of apparent undersampling and the lack of a good fit at the expected pattern speed. With the addition of data from the U28 and Voyager occultations and the revised GM for Uranus, the $m = 0$ mode was reexamined.

Figure 11 shows the results of a series of fits to the γ ring of the linear combination of an $m = 0$ mode and an inclined, precessing ellipse ($m = 1$ mode). The RMS ring-plane residual is shown as a function of the pattern speed assumed for each fit. There is a pronounced minimum at a pattern speed of 47.73198 deg hr^{-1}. The parameters of the best fit are given in Table XV, and Fig. 12 shows the individual data points and the $m = 0$ model curve. The improvement in the fit can be seen most clearly in Fig. 8, by

comparing the residuals of the γ ring from an elliptical ring model ($m = 1$ mode alone, shown in the upper panel) and the resonance orbit model (both $m = 0$ and $m = 1$, shown in the lower panel). The fit is considerably improved, but the residuals are still larger than those for the other rings. It is possible that the fit can be improved by including the $m = 6$ mode (associated with the 6:5 IER of 1986U8) as well; this is currently under investigation.

The orbital radius of a particle with an epicyclic frequency of 47.73198 ± 0.00019 deg hr^{-1} is a_{res} = 47626.24 ± 0.14 km, within 0.63 km of 47626.87 ± 0.28 km, the fitted semimajor axis of the γ ring. This close agreement strongly suggests that the fit is physically significant, and that the γ ring is undergoing radial oscillations with an amplitude of 5.15 ± 0.33 km (for a total radial excursion of 10.30 km). We point out that the ring cannot be satisfactorily modeled by an $m = 0$ mode alone (i.e., as a "breathing" *circular* ring); the precessing $m = 1$ mode must be included as well. This can be seen in Table XV, which shows that the fitted eccentricity of the γ ring is statistically significant, and is consistent with the elliptical ring model for the γ ring in Table XIV.

VI. DISCUSSION

The normal modes in the γ and δ rings can be thought of as unstable density waves, tapping their energy from viscous shear within the rings themselves. According to this view, these Lindblad resonances are not associated with shepherd satellites at all. On the other hand, the torques required to prevent the narrow Uranian rings from spreading have commonly been attributed to shepherds. Of the 10 recently discovered small satellites of Uranus, 1986U7 and 1986U8 appear to have Lindblad resonances associated with some of the rings (Porco and Goldreich 1987). They used the satellite mean motions determined by Owen and Synnott (1987) and GM for Uranus derived from Voyager data to compute resonance locations in the vicinity of the known rings. They noted that a number of resonances were located very near to the nominal locations of the rings and ring edges as determined by French *et al.* (1986a) and that a systematic shift in the ring orbital radii of 0.0124 ± 0.0021% would be sufficient to bring the locations of the resonances and the rings into accord. (Although it is not mentioned by Porco and Goldreich, this shift in the radius scale of about 6 km is very close to the quoted error of about 5 km for the semimajor axes of the rings given by French *et al.* 1986a.) With the improved ring orbits determined by the present work, we can now make a critical comparison of the computed resonance locations and the radii of ring features. The results, described below, are summarized in Table XVI.

Porco and Goldreich (1987) identified the 24:25 outer eccentric resonance (OER) or 1986U7 at 51121.2 km with the inner edge of the ε ring and the 14:13 IER of 1986U8 at 51178.1 km with the outer edge of the ring. For this identification to be correct, they required that the semimajor axis of the ε ring be 51149.7 ± 1.8 km. We obtained a fitted radius of 51149.32 ± 0.13 km, in excellent agreement with their value. This lends compelling support to the proposition that the two satellites are shepherding the ε ring, since the resonances are in precisely the right locations to provide torques in the appropriate directions to confine the ring.

As noted previously, the observed semimajor axis of the δ ring agrees almost exactly with the location associated with an $m = 2$ normal mode, as expected for a radial distortion excited by either an internal viscous overstability or parametrically by shepherding satellites (Goldreich and Tremaine 1981, Borderies *et al.* 1985, Porco and Goldreich 1987). From the observed mean width of the δ ring of 5.14 km, the outer edge is located at 48302.5 ± 0.2 km, in excellent agreement with the calculated location of the 23:22 IER of 1986U7 of 48302.5 ± 0.3 km (Porco and Goldreich

TABLE XVI

SHEPHERD SATELLITE RESONANCES

Ring	Satellite	Resonance	Feature	a_{res}	a_{obs}
ε	1986U7	24:25 OER	Inner edge	51121.2 ± 0.3	51120.3 ± 0.2
	1986U8	14:13 IER	Outer edge	51178.1 ± 1.8	51178.4 ± 0.2
1986U1R	1986U7	122:123 OER	Inner edge	50022.5 ± 0.3	50023.1 ± 0.3
δ	1986U7	23:22 IER	Outer edge	48302.5 ± 0.3	48302.5 ± 0.2
γ	1986U8	6:5 IER	Inner edge	47625.7 ± 1.8	47624.8 ± 0.4

Note. The resonance locations a_{res} are from Porco and Goldreich (1987). The observed locations of the ring edges a_{obs} were computed from ring semimajor axes in Tables XIV and XV, and mean ring widths were determined by French *et al.* (1986a) for the ε, δ, and γ rings and by Holberg *et al.* (1987) for 1986U1R. The errors in a_{obs} were determined by quadratic addition of the *tabulated* errors in the ring radii and half-widths. See text for a discussion of possible systematic errors in ring radii.

1987), confirming that 1986U7 is shepherding the outer edge of the δ ring.

We have shown that the γ ring undergoes $m = 0$ radial oscillations with an amplitude of 5.15 ± 0.33 km. It is interesting to note that this is nearly *identical* to the amplitude of its $m = 1$ mode of $ae = 5.19 \pm 0.33$ km. The possible dynamical significance of this provocative agreement has not been explored, although the amplitudes are sufficiently large that there may well be coupling between these two modes (P. Goldreich, personal communication). The 6:5 IER of 1986U8 is located at 47625.7 ± 1.8 km. Although this resonance falls close to the inner edge of the γ ring at 47624.8 ± 0.4 km (based on a mean ring width of 4.2 km), the expected wavelength of the density wave produced by this resonance is $\lambda \approx 5$ km for an assumed ring surface mass density $\Sigma \approx 10$ g cm^{-2} (see Eq. (6) of Porco and Goldreich 1987). This value is comparable to the width of the ring, so it remains possible that 1986U8 is an outer shepherd of the γ ring. A more convincing case could be made if an $m = 6$ distortion were to be detected in the ring, although the amplitude may be too small to perceive in the existing data.

Finally we confirm the association pointed out by Porco and Goldreich (1987) of the 122:123 OER of 1986U7 and the new ring 1986U1R. This ring has a fitted radius of 50023.94 ± 0.34 km and an observed width of about 1.5–2 km, putting its inner edge at 50023.1 ± 0.3 km, close to the resonance at 50022.5 ± 0.3 km. However, because of the high wavenumber and the limited observations, it is not possible to search for the $m = 123$ pattern expected from the shepherd.

The combination of new Earth-based occultation and Voyager data has enabled us to pin down the pole direction and the radius scale of the rings with much greater precision than ever before, due to the large north–south separation of the Earth-based observations and the Voyager occultation geometry. Although the formal errors of the fit are quite small, it is important to take note of a number of systematic effects which make the realistic errors somewhat larger. Possible errors in the Voyager trajectory and in the time standards of several Earth-based observations have been taken into account, as described previously. However, the orbit model used does not include the effects of motion of Uranus with respect to the system barycenter during Earth-based occultations, the forced precession of the rings by the major Uranian satellites, or the contribution of J_6 to the free precession. Furthermore, the set of ring event times used in the fit is based on square-well fits to the observed profiles, but Voyager observations show that several of

the rings are not sharp edged and have structure that varies considerably with ring longitude.

Many of these effects can be incorporated in the next generation orbit model, but in the meantime we caution against taking the error bars in Tables XIV–XVI too literally. Our best estimate is that the *absolute* radius scale of the rings is accurate to about ±1 km, comparable to the uncertainty in calculating the radial positions of resonances with 1986U7 and 1986U8 due to imprecise satellite orbital periods and the uncertainty in GM (Owen and Synnott 1987). The *relative* radii of the rings, on the other hand, are less susceptible to hidden systematic errors and are probably comparable to the errors quoted in Tables XIV and XV. The pole direction is accurate to about ±0.01°. The derived Uranus pole differs by 0.15° in right ascension and 0.04° in declination from the determination by Veillet (1983) of α (1950.0) = 76.751 ± 0.025° and δ (1950.0) = 15.066 ± 0.030°. It remains to be seen whether this substantial difference represents an interesting dynamical effect or is rather an artifact of Veillet's not having taken account of mutual secular perturbations of the satellites (Dermott and Nicholson 1986).

The gravitational harmonic coefficients J_2 and J_4 are determined in the orbit model from the apsidal precession and nodal regression rates of the rings. Since characteristic precession rates are on the order of 2 deg day^{-1}, occultation observations since the discovery of the rings in 1977 now span roughly 20 precession periods. Furthermore, since periapse longitudes have uncertainties of about 0.3° for most of the rings, it is evident that the precession rates are now known to an accuracy of order 0.3/(20 × 360), or 1 part in 24,000. The small errors quoted for J_2 and J_4 in Table XIV are a consequence of the long time baseline of observations. Realistic errors are probably somewhat larger, since higher-order coefficients and forced precessions from satellites have not been included, but it is safe to conclude that $-J_4$ is close to 2.9×10^{-5}. The significance of this to our understanding of Uranus' interior has been explored by Podolak and Reynolds (1987), who computed interior models for a range of proportions of ice and rock. *None* of their models can simultaneously match J_2 and give $-J_4$ smaller than 3×10^{-5}, and even this limit is reached only with an extremely high ice-to-rock ratio. If this conclusion is substantiated, it will require rethinking of conventional planetary accretion models to achieve such large enhancements over solar values.

VII. CONCLUSIONS

Voyager occultation timings and Earth-based observations of the occultations of U23, U25, and U28 have been added to nearly a decade of Earth-based occultation data to determine a new kinematical model for the Uranian rings. The improved orbit solution is accurate to about 1 km in the ring plane, permitting a critical comparison of ring locations and suspected resonances. The γ ring has a peculiar orbit, combining a precessing elliptical ring and a radially oscillating normal mode. The new kinematical model confirms the suspected association of resonances between the satellites 1986U7 and 1986U8 and some of the rings, as well as the suggestion that the δ ring's $m = 2$ distortion can be attributed to an excited normal mode (Porco and Goldreich 1987, Goldreich and Porco 1987). It provides compelling evidence that the 24:25 OER of 1986U7 and the 14:13 IER of 1986U8 fall exactly on the inner and outer edges of the ε ring, in just the sense required to provide confinement of the ring.

There is good reason to think that still more can be learned about the dynamics of the rings by further study of their kinematics. The midpoints of ring profiles in the best ground-based data can be fitted with square-well models with a formal precision of tens of meters. In contrast, typical post-fit orbit residuals are about *10 times larger*, on the order of a few hundred meters. If these represent true deviations from the mean ring orbits, they may be the signa-

tures of weak perturbations, perhaps due to unseen shepherd satellites or internal modes, such as those evident in the γ and δ rings. The Voyager data provide important constraints on orbital models for the rings, but they have a restricted time base and limited coverage in ring longitude; Earth-based occultations provide a long time baseline and more extensive coverage, but at limited radial resolution. Our best chance for further progress in our understanding of the Uranian ring system lies in taking advantage of the complementary nature of these observations and in a vigorous observing program of Earth-based ring occultations.

ACKNOWLEDGMENTS

The observations described in this paper were acquired and analyzed through the efforts and cooperation of many people. We thank R. Baron for the design and construction of the portable clocks, E. W. Dunham for assistance in preparing for the observations, and E. Erickson for the use of an IR dewar. B. Gregory and R. Smith are responsible for the excellent performance of the infrared system at CTIO. M. Frueh assisted with the observations at McDonald Observatory, and D. Griep assisted with the IRTF observations of U28. W. Tittemore developed the software to perform the deconvolutions, and J. Wiseman, S. Levine, and J. Kim assisted with the data analysis as part of MIT's Undergraduate Research Opportunities Program. R. Cesarone, of the Voyager Navigation Team, provided us with the Voyager trajectory information, and M. Standish supplied the DE-125 ephemeris. We also thank G. L. Tyler and R. A. Simpson for providing us with unpublished opacity profiles from the Voyager Radio Science Experiment and L. Esposito, L. Horn, and A. L. Lane for their tabulations of the PPS ring occultation event times. P. Nicholson, D. Gresh, and P. Rosen provided independent occultation event calculations which were used to test the code used for the final orbit fits. We appreciate the help of the technical staff of Haystack Observatory for assistance with timing calibrations. C. Porco helped to clarify a number of points regarding resonances and normal modes. The Carlos Sanchez Telescope, on the island of Tenerife, is operated by the Instituto de Astrofisica de Canarias and its Observatorio del Teide. This research was supported in part by NASA Grants NAGW 656,NAGW 610, NSG 7256 and by NSF Grant AST 8519518.

REFERENCES

BARON, R. L., E. W. DUNHAM, AND J. L. ELLIOT 1983. A portable telescope, photometer, and data-recording system. *Publ. Astron. Soc. Pac.* **95,** 925–937.

BORDERIES, N., P. GOLDREICH, AND S. TREMAINE 1985. A granular flow model for dense planetary rings. *Icarus* **63,** 406–420.

DERMOTT, S., AND P. NICHOLSON 1986. The masses of the uranian satellites. *Nature* **319,** 115–120.

ELLIOT, J. L., R. G. FRENCH, K. J. MEECH, AND J. H. ELIAS 1984. Structure of the Uranian rings. I. Square-well model and particle-size constraints. *Astron. J.* **89,** 1587–1603.

ELLIOT, J. L., AND P. D. NICHOLSON 1984. Rings of Uranus. In *Planetary Rings* (R. Greenberg and A. Brahic, Eds.). Univ. of Arizona Press, Tucson.

FRENCH, L. M., G. MORALES, A. S. DALTON, J. J. KLAVETTER, AND S. R. CONNER 1985. Photometry of occultation candidate stars. I. Uranus 1985 and Saturn 1985–1991. *Astron. J.* **90,** 668–669.

FRENCH, L. M., G. MORALES, S. L. GAISER, AND J. FROGEL 1986. Photometry of occultation candidate stars. II. Uranus 1985–1990 and Saturn 1986–1991. *Icarus* **67,** 540–542.

FRENCH, R. G., J. L. ELLIOT, AND S. E. LEVINE 1986a. Structure of the Uranian rings. II. Ring orbits and widths. *Icarus* **67,** 134–163.

FRENCH, R. G., J. A. KANGAS, AND J. L. ELLIOT 1986b. What perturbs the γ and δ rings of Uranus? *Science* **231,** 480–483.

GOLDREICH, P., AND C. PORCO 1987. Shepherding of the Uranian rings. II. Dynamics. *Astron. J.* **93,** 730–737.

GOLDREICH, P., AND S. TREMAINE 1981. The origin of the eccentricities of the rings of Uranus. *Astrophys. J.* **243,** 1062–1075.

HOLBERG, J. B., P. D. NICHOLSON, R. G. FRENCH, AND J. L. ELLIOT 1987. Stellar occultation probes of the Uranian rings at 0.1 and 2.2 μm: A comparison of Voyager Ultraviolet Spectrometer and Earth-based results. *Astron. J.* **94,** 178–188.

KLEMOLA, A. R., D. J. MINK, AND J. L. ELLIOT 1981. Predicted occultations by Uranus: 1981–1984. *Astron. J.* **86,** 138–140.

LANE, A. L., C. W. HORD, R. A. WEST, L. W. ESPOSITO, K. E. SIMMONS, R. M. NELSON, B. D. WALLIS, B. J. BURATTI, L. J. HORN, A. L. GRAPS, AND W. R. PRYOR 1986. Photometry from Voyager 2: Initial results from the Uranian atmosphere, satellites, and rings. *Science* **233,** 65–70.

MILLIS, R. L., L. H. WASSERMAN, AND R. G. FRENCH 1987. Observations of the 22 April 1982 stellar occultation by Uranus and the rings. *Icarus* **69,** 176–184.

MINK, D. J., AND A. KLEMOLA 1985. Predicted occultations by Uranus, Neptune, and Pluto: 1985–1990. *Astron. J.* **90,** 1894–1899.

OWEN, W. M., JR., AND S. P. SYNNOTT 1987. Orbits of the ten small satellites of Uranus. *Astron. J.* **93,** 1268–1271.

PODOLAK, M., AND R. T. REYNOLDS 1987. The rota-

tion rate of Uranus, its internal structure and the process of planetary accretion. *Icarus* **70,** 31–36.

PORCO, C. C., AND P. GOLDREICH 1987. Shepherding of the Uranian rings. I. Kinematics. *Astron. J.* **93,** 724–729.

SMITH, B. A., L. A. SODERBLOM, R. BEEBE, D. BLISS, J. M. BOYCE, A. BRAHIC, G. A. BRIGGS, R. H. BROWN, S. A. COLLINS, A. F. COOK II, S. K. CROFT, J. N. CUZZI, G. E. DANIELSON, M. E. DAVIES, T. E. DOWLING, D. GODFREY, C. J. HANSEN, C. HARRIS, G. E. HUNT, A. P. INGERSOLL, T. V. JOHNSON, R. J. KRAUSS, H. MASURSKY, D. MORRISON, T. OWEN, J. B. PLESCIA, J. B. POLLACK, C. PORCO, K. RAGES, C. SAGAN, E. M. SHOEMAKER, L. A. SROMOVSKY, C. STOKER, R. G. STROM, V. E. SUOMI, S. P. SYNNOTT, R. J. TERRILE, P. THOMAS, W. R. THOMPSON, AND J. VEVERKA 1986. Voyager 2 in the Uranian system: Imaging science results. *Science* **233,** 43–64.

STANDISH, E. M., AND J. K. CAMPBELL 1984. The masses of the outer planets. *Bull. Amer. Astron. Soc.* **16,** 722.

TYLER, G. L., D. N. SWEETNAM, J. D. ANDERSON, J. K. CAMPBELL, V. R. ESHELMAN, D. P. HINSON, G. S. LEVY, G. F. LINDAL, E. A. MAROUF, AND R. A. SIMPSON 1986. Voyager 2 radio science observations of the Uranian system: Atmosphere, rings, and satellites. *Science* **233,** 79–84.

VEILLET, C. 1983. *De l'observation et du mouvement des satellites d'Uranus.* Thesè de Doctorat d'Etat, Université de Paris 6.